

NUCLEAR DATA AND MEASUREMENTS SERIES

ANL/NDM-37

Neutron Inelastic Scattering Studies for Lead-204

by

D.L. Smith and J.W. Meadows

December 1977

**ARGONNE NATIONAL LABORATORY,
ARGONNE, ILLINOIS 60439, U.S.A.**

NUCLEAR DATA AND MEASUREMENTS SERIES

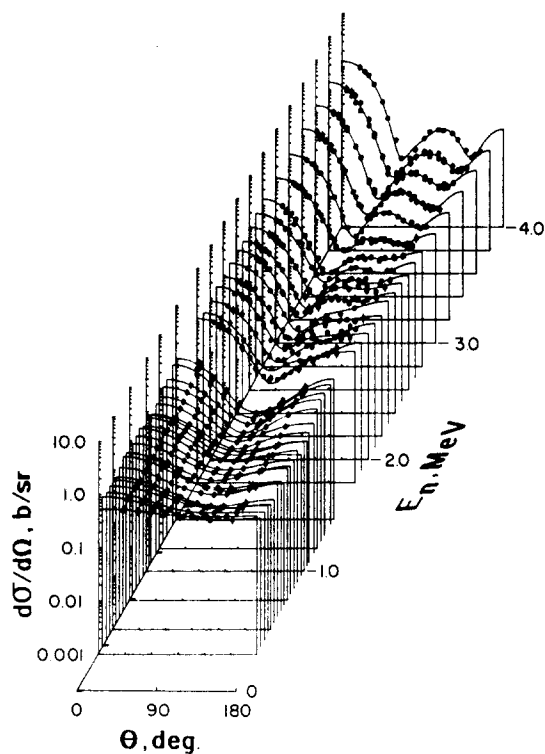
ANL/NDM-37

NEUTRON INELASTIC SCATTERING
STUDIES FOR LEAD-204

by

D. L. Smith and J. W. Meadows

December 1977



U of C AUA USERDA

ARGONNE NATIONAL LABORATORY,
ARGONNE, ILLINOIS 60439, U.S.A.

The facilities of Argonne National Laboratory are owned by the United States Government. Under the terms of a contract (W-31-109-Eng-38) between the U. S. Atomic Energy Commission, Argonne Universities Association and The University of Chicago, the University employs the staff and operates the Laboratory in accordance with policies and programs formulated, approved and reviewed by the Association.

MEMBERS OF ARGONNE UNIVERSITIES ASSOCIATION

The University of Arizona
Carnegie-Mellon University
Case Western Reserve University
The University of Chicago
University of Cincinnati
Illinois Institute of Technology
University of Illinois
Indiana University
Iowa State University
The University of Iowa

Kansas State University
The University of Kansas
Loyola University
Marquette University
Michigan State University
The University of Michigan
University of Minnesota
University of Missouri
Northwestern University
University of Notre Dame

The Ohio State University
Ohio University
The Pennsylvania State University
Purdue University
Saint Louis University
Southern Illinois University
The University of Texas at Austin
Washington University
Wayne State University
The University of Wisconsin

NOTICE

This report was prepared as an account of work sponsored by the United States Government. Neither the United States nor the United States Atomic Energy Commission, nor any of their employees, nor any of their contractors, subcontractors, or their employees, makes any warranty, express or implied, or assumes any legal liability or responsibility for the accuracy, completeness or usefulness of any information, apparatus, product or process disclosed, or represents that its use would not infringe privately-owned rights.

ANL/NDM-37

NEUTRON INELASTIC SCATTERING
STUDIES FOR LEAD-204

by

D. L. Smith and J. W. Meadows

December 1977

In October 1977, the U. S. Energy Research and Development Agency (ERDA) was incorporated into the U. S. Department of Energy. The research and development functions of the former U. S. Atomic Energy Commission had previously been incorporated into ERDA in January 1975.

Applied Physics Division
Argonne National Laboratory
9700 South Cass Avenue
Argonne, Illinois 60439
U.S.A.

NUCLEAR DATA AND MEASUREMENTS SERIES

The Nuclear Data and Measurements Series presents results of studies in the field of microscopic nuclear data. The primary objective is the dissemination of information in the comprehensive form required for nuclear technology applications. This Series is devoted to: a) measured microscopic nuclear parameters, b) experimental techniques and facilities employed in measurements, c) the analysis, correlation and interpretation of nuclear data, and d) the evaluation of nuclear data. Contributions to this Series are reviewed to assure technical competence and, unless otherwise stated, the contents can be formally referenced. This Series does not supplant formal journal publication but it does provide the more extensive information required for technological applications (e.g., tabulated numerical data) in a timely manner.

TABLE OF CONTENTS

| | Page |
|--|------|
| ABSTRACT. | 1 |
| I. INTRODUCTION. | 2 |
| II. ACTIVATION OF THE 66.9-M ISOMERIC STATE BY NEUTRON INELASTIC SCATTERING. | 5 |
| A. Experimental Procedures | 5 |
| B. Data Processing | 8 |
| C. Results and Discussion. | 10 |
| III. PROMPT GAMMA RADIATION FROM NEUTRON INELASTIC SCATTERING. | 12 |
| A. Experimental Procedures | 12 |
| B. Data Processing | 14 |
| C. Results and Discussion. | 16 |
| IV. SURVEY OF AVAILABLE FAST-NEUTRON CROSS SECTION DATA FOR LEAD-204 . | 23 |
| V. SUMMARY. | 26 |
| APPENDIX A: NEUTRON SCATTERING CALCULATIONS FOR COAXIAL CYLINDER GEOMETRIES | 27 |
| REFERENCES. | 33 |
| TABLES. | 36 |
| FIGURES | 54 |

NEUTRON INELASTIC SCATTERING
STUDIES FOR LEAD-204*

by

D. L. Smith and J. W. Meadows

Argonne National Laboratory
9700 South Cass Avenue
Argonne, Illinois 60439
U.S.A.

ABSTRACT

A 9.57-g sample of lead metal, enriched to 99.7% ^{204}Pb , has been used in an investigation of neutron inelastic scattering from this rare isotope at the Argonne National Laboratory Fast-Neutron Generator Facility. Neutron excitation of the 66.9-m isomeric state at 2.186 MeV in ^{204}Pb has been measured from near threshold to ~ 10 MeV using activation techniques. Cross sections and a value for the isomeric half life have been derived from these data. Time-of-flight techniques were employed to measure spectra of promptly-emitted gamma rays from the $^{204}\text{Pb}(n;n',\gamma)^{204}\text{Pb}$ reaction at neutron energies ≤ 3 MeV. Cross sections and angular distributions have been derived from these data for several of the stronger transitions. Other available fast-neutron data for this isotope are reviewed briefly in this report.

*This work is supported by the U. S. Department of Energy.

I. INTRODUCTION

The isotope ^{204}Pb is the least-abundant (~1.4%) stable isotope of elemental lead [1]. Consequently, the interactions of fast-neutrons (>0.1 MeV) with ^{204}Pb are of little interest for most applications concerned with elemental lead (especially those involving the total cross section or elastic and inelastic scattering processes). Because of low abundance, the contributions from ^{204}Pb were either ignored or treated in an approximate fashion in the preparation of the ENDF/B-IV File for lead [2,3]. A quick survey of the available neutron data for ^{204}Pb [4,5] indicates that the data base for this isotope is very limited and unbalanced. This data base will be reviewed briefly in Section IV. Clearly there is insufficient experimental data available for a comprehensive evaluation of ^{204}Pb without extensive recourse to theoretical computations.

There are some specialized applications for ^{204}Pb neutron data, particularly those corresponding to the $^{204}\text{Pb}(n;n')^{204\text{m}}\text{Pb}$ (66.9m) and $^{204}\text{Pb}(n;2n)^{203}\text{Pb}$ reactions, because of the induced radioactivity. A request for cross section data on $^{204}\text{Pb}(n;n')^{204\text{m}}\text{Pb}$ was included in a 1973 compilation of cross section data requests prepared by the U. S. Nuclear Data Committee of the U. S. Atomic Energy Commission [6]. This request, and the availability of a lead sample which is highly enriched in ^{204}Pb , prompted the current study.

^{204}Pb is an interesting nucleus from the point of view of nuclear structure. ^{208}Pb is doubly magic, therefore, the structure of ^{204}Pb results from the interaction of four neutron holes with each other and with the ^{208}Pb core. Shell model calculations have been carried out for this nucleus as well as for ^{206}Pb and ^{212}Pb (e.g., Refs. 7 and 8). The available information on the levels of ^{204}Pb appears to have originated predominantly from experimental studies of the decay of ^{204}Bi , the $^{206}\text{Pb}(p,t)^{204}\text{Pb}$ reaction, the inelastic scattering of

alpha particles and deuterons, the $^{205}\text{Tl}(p;2n\gamma)^{204}\text{Pb}$ reaction and the $^{203}\text{Tl}(\alpha;t)^{204}\text{Pb}$ reaction (e.g., Ref. 9). Neutron nuclear data on the levels of ^{204}Pb is unavailable. It is easy to see why. The abundance of ^{204}Pb in elemental lead is so low that most neutron experiments are not feasible with elemental samples. Furthermore, the quantity of separated ^{204}Pb available is limited and is inadequate for many neutron experiments.

The $^{204}\text{Pb}(n;n')^{204\text{m}}\text{Pb}$ reaction can be studied (well above threshold) with activation methods using natural lead samples, because the gamma-ray spectrum for the decay of $^{204\text{m}}\text{Pb}$ is well known (e.g., Refs. 10, 11, and 12). However, to perform measurements very near to threshold, it is necessary to use an enriched sample. A 9.57-g sample of metallic lead, enriched to 99.7% ^{204}Pb , was obtained on loan from Oak Ridge National Laboratory [13]. The specifications for this sample appear in Table 1.

The sample is ideal for studies of activation of $^{204\text{m}}\text{Pb}$ with monoenergetic neutrons, and could undoubtedly be used for studies of the $^{204}\text{Pb}(n;2n)^{203}\text{Pb}$ by the activation method - although the latter measurements were not made during the present study. The sample is not adequate for total, direct neutron scattering, or $(n;\gamma)$ cross section measurements involving conventional experimental techniques. Since an experimental facility is available at Argonne for conventional $(n;n'\gamma)$ measurements [14], it was decided to attempt some gamma-ray production cross section measurements even though the sample is far smaller than the ideal size. Researchers at the University of Alberta [15] have developed a technique for performing $(n;n'\gamma)$ studies using small samples such as the ^{204}Pb sample presently available. Their approach relies heavily on a combination of theory and experiment and has as its goal the determination of spins and parities for nuclear levels involved in the observed transitions. However, the method does not specifically provide absolute cross section values, so a collaborative

effort is in progress for the $^{204}\text{Pb}(n;n'\gamma)^{204}\text{Pb}$ reaction involving one of the authors (DLS) and researchers at the University of Alberta. Preliminary measurements have been performed on ^{204}Pb in Alberta, but this work is not finished and will be reported later when completed. The results from this research program should yield information which will compliment the cross section data obtained from the present work.

This report is divided into five sections. The experiment undertaken to measure cross sections for production of the 66.9-m isomer by neutron inelastic scattering is discussed in Section II. The experiment conducted at Argonne to measure prompt gamma-ray spectra and cross sections for the $^{204}\text{Pb}(n;n'\gamma)^{204}\text{Pb}$ reaction is discussed in Section III. In Section IV, the status of the neutron nuclear data base for ^{204}Pb is reviewed. Finally, the results of the present work are summarized in Section V.

II. ACTIVATION OF THE 66.9-M ISOMERIC STATE BY NEUTRON INELASTIC SCATTERING

A. Experimental Procedures

The experimental procedures used for the present activation experiment closely resembled those described in detail in earlier reports [16-19]. Highlights of the general method and specific details relevant to the $^{204}\text{Pb}(n;n')^{204\text{m}}\text{Pb}$ reaction are included here. Furthermore, a new procedure was used for computation of neutron scattering corrections. It represents an improvement over the approach described in Ref. 17. The method is discussed in Section II.B and in Appendix A.

The ^{204}Pb -enriched sample described in Section I and Table 1 was used in the present measurements along with several metallic elemental lead samples, each having approximately the same mass and dimensions as the ^{204}Pb -enriched sample. The batch of elemental lead from which these samples were fabricated was subjected to a spectrochemical analysis to determine impurities and a mass spectrometric analysis to establish the isotopic abundance of ^{204}Pb . The latter analysis is especially important since the abundance of ^{204}Pb is low and may vary somewhat depending on the origin of the lead. The results of these analyses appear in Table 2.

During irradiation, each sample was fastened to a low-mass fission detector which served as the neutron-fluence monitor [20]. This ionization chamber was made from a cylindrical steel can with 0.025-cm-thick walls. The samples were placed outside the chamber; the backing plates with uranium deposits were mounted inside the chamber adjacent to the samples, as shown in Fig. 1. Methane at 1 atm served as the gaseous medium for the ionization chamber. A discriminator was used to reject noise and alpha pulses; pulses above the discrimination level were recorded as fission events in the detector.

Spectra from the fission detector were also recorded in order to guard against loss of data due to spurious noise pulses and to provide information needed in the determination of corrections.

Two uranium deposits were used in the measurements. One of the deposits was enriched in ^{235}U and it was used predominantly for measurements near threshold ($E_n \leq 4$ MeV); the second deposit was enriched in ^{238}U and it was used predominantly for measurements at higher energies. However, measurements were also made at several energies using both monitor deposits to insure data consistency. The uranium deposits were 2.54 cm in diameter and were fabricated by evaporating UF_4 , isotopically enriched in ^{235}U or ^{238}U , onto thin metal backing plates. The isotopic contents of these materials were determined by mass spectrographic analysis; the quantity of uranium in each deposit was deduced from measurement of the specific alpha activities according to previously described procedures [17, 21, 22]. The specifications for these two deposits appear in Table 3.

Elemental lead samples and the ^{204}Pb -enriched sample were used in measurements at neutron energies >2.6 MeV while measurements at lower energies were made exclusively with the ^{204}Pb -enriched sample. The ^{204}Pb -enriched sample was irradiated on several occasions at ~ 10 MeV in order to produce sufficient activity for measurements of the half life and for coincidence counting measurements to calibrate the gamma-ray detector.

Neutrons with energies <5.3 MeV were produced via the $^7\text{Li}(p;n)^7\text{Be}$ reaction. Natural lithium metal was evaporated onto tantalum cups to make these targets. Neutrons with energies in the range 5-10 MeV were produced via the $\text{D}(d;n)^3\text{He}$ reaction. A 2-cm-long gas cell containing deuterium gas at 2 atm (see Fig. 1) was used for a target. The sample and fission detector were placed on the beam axis 3 to 4 cm from the target for these measurements

(see Fig. 1). There are variations in the experimental techniques associated with use of these two types of targets. The neutron spectrum from the lithium target is complex at higher energies because of the presence of neutrons from the ${}^7\text{Li}(p;n){}^7\text{Be}$ and ${}^7\text{Li}(p;n{}^3\text{He}){}^4\text{He}$ reactions. The presence of neutrons from the $\text{D}(d;np)\text{D}$ reaction complicates the neutron spectrum from the deuterium source at higher energies. Methods for coping with these problems have been reported [16-18]. Background measurements were performed during irradiations made using both lithium and deuterium targets to determine the effects of neutrons from the tantalum cups and empty gas-target assembly, respectively.

The production of ${}^{204m}\text{Pb}$ was determined from measurements of the characteristic decay gamma radiation with an $\sim 50\text{-cm}^3$ true-coaxial $\text{Ge}(\text{Li})$ detector. Samples were placed close to this detector in a holder designed for this purpose. Figure 2 is typical of spectra obtained in this fashion. Data needed for a determination of the half life were acquired by following the decay of the ${}^{204}\text{Pb}$ -enriched sample, for a time period exceeding ten half lives, following one of the irradiations. The ${}^{204}\text{Pb}$ -enriched sample was reused many times. It was necessary to allow the ${}^{204m}\text{Pb}$ activity to die away to a negligible level after each exposure prior to re-use. A 24-hour interval was found to be completely adequate for this purpose (decay factor $\sim 5 \times 10^{-10}$).

The decay of ${}^{204m}\text{Pb}$ is shown schematically in Fig. 3 [9]. Only the 0.37474-, 0.89915-, and 0.9117-MeV gamma rays were seen in the spectra (e.g., Fig. 2). A peak corresponding to coincidence summing of the 0.3747-MeV gamma rays and the higher-energy gamma rays was seen in all spectra because the samples were counted in close proximity to the $\text{Ge}(\text{Li})$ detector. Because of the large probability for absorption of gamma rays in lead, it was desirable to calibrate the gamma ray detector with a standard source of ${}^{204m}\text{Pb}$ activity distributed in a sample similar to those used for the cross-section measurements. In this fashion, it was possible to avoid the computation of absorption

corrections for the gamma rays. A standard source of ^{204}mPb activity was prepared by irradiating the ^{204}Pb -enriched sample with neutrons and then determining the absolute source strength of this sample by means of standard coincidence-counting techniques [17, 23, 24]. A second Ge(Li) detector was used, along with the first, for gamma-gamma coincidence counting. Several coincidence-count and singles-count measurements were made in order to obtain the data need for calibration of the primary Ge(Li) detector. It was necessary to reactivate the source used in standardization several times because of the relatively short half life (66.9 m) involved. The standardized source was counted several times in the geometry used for counting during the cross-section measurements.

B. Data Processing

Gamma-ray full-energy peak yields were deduced from measured spectra. The yields of 0.89915- and 0.9117-MeV gamma rays were used in determining cross sections and for determining a value for the half life. The half life was found by least-squares fitting of an exponential decay curve to data representing unit time yield (corrected for deadtime) plotted vs. decay time.

Cross sections for the reactions studied were computed relative to ^{235}U and ^{238}U fission cross sections after correcting the data for various experimental effects. ENDF/B-IV evaluated ^{235}U and ^{238}U fission cross sections and cross sections for neutrons in elemental lead were used in this analysis and throughout the work described in this report [25]. Photon cross sections for lead were obtained from an evaluation by Storm and Israel [26].

Corrections for neutron-source properties were deduced from data obtained from measurements made in our laboratory [16-18] and from a paper by Liskien and Paulsen [27]. The raw data were corrected, where required, for sample activity and monitor fissions produced by neutrons from bare target assemblies.

Corrections were made to account for geometric factors and the effects of neutron absorption and scattering. Neutron-scattering corrections were limited to single-scattering events since higher orders were estimated to be negligible. The scattering corrections are shown symbolically in Fig. 4. "Alpha" designates activations produced by neutrons which have scattered in the sample. "Beta" designates activations produced by neutrons which have scattered from various parts of the fission detector and target assembly. "Gamma" designates fissions produced by neutrons which have scattered in the sample. "Rho" designates fissions produced by neutrons which have scattered in the fission detector and target assembly. All correction factors were neutron-energy dependent. A Monte-Carlo computer program (CYSCAT), which has been developed by one of the authors (JWM), was used in the neutron scattering calculations. This code is described in Appendix A. Both elastic and inelastic scattering processes were considered in the calculations. Computed values for the scattering corrections are presented in Table 4.

Raw fission counts were corrected for deposit-thickness effects, thermal background (for ^{235}U monitor) and loss of low-pulse-height fission events rejected along with electronic noise and alpha pulses by a discriminator.

Raw sample-count data were corrected for decay half life and other essential time factors. Corrections for sum coincidences, gamma-ray absorption, geometrical factors, internal conversion and properties of $^{204\text{m}}\text{Pb}$ decay all are contained in the counting efficiency. Monte-Carlo methods were used in the analysis procedures.

The application of various corrections and computation of reaction cross sections were carried out for the most part with the aid of a digital computer. Therefore, it was possible to investigate in detail the sensitivity of the computed cross sections to the various applied corrections.

The energy resolution for these measurements was governed by target thickness and kinematic broadening. Kinematic broadening was the dominant factor in measurements with the deuterium-gas target. Generally, the neutron-energy resolution was 0.06-0.17 MeV for the lithium target measurements and 0.3-0.4 MeV for deuterium-target measurements.

Uncertainties in the measured cross sections can be attributed to statistics as well as to a variety of other experimental factors. Known systematic uncertainty amounted to $\sim 7\%$ for these measurements. This was combined with the statistical uncertainties in quadrature in order to obtain the total reported errors for the measured cross section ratios. Table 5 indicates the relative importance of some of the identified sources of uncertainty in our data. Detector count errors were relatively unimportant except for measurements near threshold.

C. Results and Discussion

The data from the present work yield a value of 67.2 m ($\pm 1.3\%$) for the half life of ^{204}mPb . This differs by only 0.4% from the value 66.9 m appearing in the Nuclear Data Sheets [9] and is therefore consistent with this adopted value.

Measured cross section ratios and calculated cross sections appear in Table 6. These cross sections for the $^{204}\text{Pb}(n;n')^{204}\text{Pb}$ reaction are plotted in Fig. 5 along with other differential values from the literature [28-31]. Comparison of results from the present work with other reported values is not very meaningful since the cross sections from the present work correspond to energies below ~ 10 MeV while the only other available monoenergetic cross sections are for energies above ~ 13 MeV. When all these data are considered together, however, it becomes possible to define a fairly reliable excitation function for this reaction from threshold to ~ 20 MeV based only on experimental

values. An eyeguide was sketched through these points and an interpolated estimate was provided for the region from 10 to 13 MeV where no data are available. The cross section for production of ^{204m}Pb decreases rapidly above ~ 10 MeV, largely as a result of considerable (n;2n) competition as will be discussed in Section IV. The eyeguide is shown in Fig. 5, and it can be generated by linear interpolation using values provided in Table 7.

Calamand has published a review of ^{235}U fission-spectrum-average cross sections for many reactions including the $^{204}\text{Pb}(n;n')^{204}\text{Pb}$ reaction [32]. Three experimental values were included in this evaluation [33-35]. The recommended value is 0.0186 ± 0.0015 barn [32]. We integrate our eyeguide cross section (Table 7) spectrum using a Maxwellian ^{235}U fission spectrum with a temperature of 1.32 MeV as defined for the ENDF/B-IV Dosimetry File [36]. This analysis led to a value of 0.017 ($\pm 11\%$) for the spectrum-average cross section. The estimated error is based on an assumption of $\sim 8\%$ error in the differential cross section ratio, $\sim 5\%$ uncertainty in the fission neutron spectrum shape and $\sim 5\%$ uncertainty in the monitor cross sections. The average cross section computed from differential information differs by $\sim 9\%$ from the evaluated integral value of Calamand; so the two results are consistent within the estimated errors.

The calculation of the spectrum-average cross section was performed using code SENSY [37]. This code yields other results which are useful in understanding the spectrum-average result (see Fig. 6). For example, the region above ~ 10 MeV contributes only $\sim 2\%$ to the spectrum average. Therefore, we have essentially a direct comparison of the data from the present experiment and the available integral data.

III. PROMPT GAMMA RADIATION FROM NEUTRON INELASTIC SCATTERING

As indicated in Section I, the available ^{204}Pb -enriched lead sample is too small to provide the desired sensitivity for $(n;n'\gamma)$ measurements using the facility available in this laboratory [38]. However, because of the unique nature of the sample and the absence of $(n;n'\gamma)$ data for ^{204}Pb , it was decided to perform some measurements in spite of this shortcoming.

As an aid in identification of transitions, the level scheme adopted for the Nuclear Data Sheets [9] was reviewed and all energetically possible transitions (without regard to physical limitations imposed by spin-parity selection rules) between these assumed levels were determined. This information proved very helpful in identifying the probably origin of several gamma ray lines observed in the measured spectra.

A. Experimental Procedures

The apparatus and procedures for the present experiment have been described in earlier reports [38-40]. The experimental procedures were modified slightly in order to optimize the quality of the data acquired with the small sample or to account for some differences in the geometry. These exceptions will be indicated in the following text.

The neutron source for the present measurements was the $^7\text{Li}(p;n)^7\text{Be}$ reaction. The characteristic neutron spectrum for this source is described in an earlier report [16]. Pulsed and bunched proton beams were obtained from the Argonne National Laboratory Fast-Neutron Generator. Average beam intensities of $\sim 5 \mu\text{A}$ on target were obtained with a pulse rate of $\sim 2 \text{ MHz}$ and time resolution of $\sim 1 \text{ nanosecond}$. Neutron-energy resolution was primarily dependent upon the thickness of the natural lithium metal deposits which were evaporated onto tantalum backings and used as targets. The average resolution was $\sim 0.12 \text{ MeV}$.

The ^{204}Pb -enriched sample was placed 12.6 cm from the neutron source at zero degrees. The axis of the sample was coincident with the beam axis during most of the irradiations. A few irradiations were made with the sample closer to the neutron source to obtain enough yield for identification of weak transitions, or with the sample tilted at an angle, to facilitate measurement of angular distributions.

The neutron fluence was measured with a fission detector which contained a 2.54-cm diameter deposit of 2.523×10^{18} atoms of uranium. The isotopic composition of this deposit is: ^{234}U (0.9%), ^{235}U (93.3%), ^{236}U (0.3%) and ^{238}U (5.5%). The fission detector was placed on the beam line between the neutron source and the sample. The distance from the neutron source to the uranium deposit was 4.3 cm. Since calibration of the apparatus was sensitive to the distances from the neutron source to the sample and to the fission detector, these distances were measured with a micrometer and were rechecked periodically during the experiment.

Because of the small sample size, and the potential for spectral interference by the fission chamber, the sample irradiations and fission-detector (primary monitor) irradiations were performed successively, rather than simultaneously, under conditions which were as nearly constant as possible. Three secondary monitors were used to check on the constancy of the irradiation conditions and to measure relative fluence; these were:

- i) a beam-current integrator,
- ii) a small plastic scintillator,
- iii) a BF_3 long counter.

Intercomparison of data from these monitors indicated uncertainties of <1% in relative fluence measurements for all the irradiations.

The gamma radiation produced by fast-neutron bombardment of the lead sample was measured with an $\sim 60\text{-cm}^3$ true-coaxial Ge(Li) detector. This detector was placed in a shield which pivots around the sample position through the angular range 30-135 degrees. The relative full-energy peak efficiency for this detector was measured using a series of radioactive gamma-ray sources, including ^{56}Co , ^{60}Co , ^{22}Na , ^{152}Eu , ^{133}Ba , etc., over the range $E_\gamma = 0.1\text{-}3.5$ MeV [38]. The absolute efficiency was measured at 0.662, 1.274, and 1.333 MeV using U. S. National Bureau of Standards calibrated ^{137}Cs , ^{22}Na , and ^{60}Co sources placed at the sample position.

Excitation functions were measured with the detector at ~ 125 degrees. The neutron fluence was measured at each energy during this portion of the experiment. Angular distribution measurements were performed at neutron energies of 1.037, 1.23, and 1.432 MeV. There was no need to measure absolute neutron fluence in this part of the experiment, so only the secondary monitors were employed.

The experimental apparatus is shown in Fig. 7. All measurements were performed at neutron energies ~ 3 MeV. Background (no sample) runs were made at all energies to ensure proper identification of gamma rays from the sample.

Time-of-flight techniques were used to reduce time-uncorrelated background, and the experimental data were recorded with an on-line computer system [38,41]. Gamma-ray pulse-height spectra, time-of-flight spectra for the gamma-ray detector, fission detector and scintillation detector, as well as integrator and long counter counts were stored in the computer.

B. Data Processing

Figure 8 shows the prompt gamma-ray spectrum for $E_n \sim 3$ MeV. Twenty-five gamma-ray full-energy peaks, not present in the background measurements, were observed at this energy. The energies of the gamma rays were deduced from a calibration of the spectrometer (established using sources of well-known gamma-ray lines). The counts in the full-energy peaks were obtained after subtraction of

background. The monitor counts were obtained from the appropriate peaks in the time-of-flight spectra whenever the fission detector (or scintillation detector) served as the monitor. The time condition which had to be satisfied in order for the gamma-rays detected to be recorded as prompt events corresponded to a window of ~ 63 nanoseconds. The gamma-ray time peak exhibited a resolution of ~ 6 nanoseconds, but there was considerable time straggling evident--particularly for low-energy gamma rays. The time "window" closed ~ 40 nanoseconds after the arrival of the majority of the prompt gamma rays (center of the time peak). Owing to the presence of another quasi-isomeric level ($0.29 \mu\text{sec}$) at 1.2739-MeV excitation in ^{204}Pb , only part of the excitation strength was observed for several of the gamma rays measured in this experiment.

The computation of cross sections from the measured quantities is complicated because of numerous experimental details which must be considered. These include geometry, secondary neutron groups from the source reaction, lithium-target thickness, the absorption and scattering of neutrons and gamma rays, and thermal-neutron fission corrections. The formalism for these calculations is described in Refs. 39 and 40. Minor modifications in the methods were incorporated to account for peculiarities of the present geometry. Neutron-scattering calculations were not made per se. Instead, the approximation of Day [39,42] was employed to account for the combined effects of absorption and scattering of neutrons. A similar approach was used to account for absorption and coherent scattering of the gamma rays.

The measured quantities were ratios of gamma-ray production cross sections to ^{235}U fission cross sections. Because of the low sensitivity of this experiment, the dominant source of experimental error was the uncertainty in gamma-ray yield. An estimated systematic error of $\sim 6\%$ is also included for the ratio

measurements. The sources of systematic error are listed in Table 8. The systematic and statistical errors were treated as uncorrelated in determining the total errors for the ratios.

C. Results and Discussion

The observed transitions (not present in background spectra) are given in Table 9. Figure 9 shows the probable origin of several of these transitions. The identification of those shown with dashed lines is speculative because of limited evidence. Ten of the observed gamma rays do not fit into the adopted level scheme [9] so they are not shown in Fig. 9. These gamma rays may correspond to transitions involving unknown levels in ^{204}Pb , but the information available from the present work is not adequate to permit identification of any new levels in this nucleus.

The measured cross-section ratios and cross sections for excitation of several of the transitions observed in the present work are given in Table 10 and in Figs. 10 and 11. These are angle-integrated cross sections which were computed using the expression

$$\sigma \approx 4\pi \left. \frac{d\sigma}{d\Omega} \right|_{125^\circ} \quad (1)$$

It is known that gamma-production differential cross sections can be expressed as Legendre polynomial expansions involving only even-order terms [43]. Equation (1) is valid provided that fourth- and higher-order terms are negligible. Since these terms are expected to be small and the errors in the measured cross section ratios are fairly large, it is reasonable to neglect them. The approximation represented by Eq. (1) is not always acceptable (e.g., see Refs. 40 and 44 which deal with the $^{56}\text{Fe}(n;n'\gamma)^{56}\text{Fe}$ reaction).

The cross sections given in Table 10 and Figs. 10 and 11 were computed from the measured ratios. The indicated errors are ratio errors only and do

not include uncertainties in the ^{235}U fission cross section which served as a standard.

The only gamma-ray with sufficient yield for angular distribution measurements was the 0.8994-MeV transition. Angular distributions were measured at neutron energies of 1.037, 1.23 and 1.432 MeV. The results appear in Table 11 and Fig. 12.

These angular distributions were fitted with Legendre-polynomial expansions up to order four. No improvement in the fits were obtained for expansions beyond second order. Values for w_2 -coefficients, defined by

$$(\frac{d\sigma}{d\Omega}) = (\sigma/4\pi)[1 + w_2P_2(\cos\theta)], \quad (2)$$

appear in Table 12.

Next we review the specific transitions and indicate how they relate to the structure of ^{204}Pb . All twenty-five transitions observed probably originate from neutron interactions with ^{204}Pb since they are not present in any background spectra. Table 9 and Figs. 8-11 supplement the following descriptive material.

Transition 1: 0.2894 MeV

The threshold for exciting this gamma ray is below 2-MeV neutron energy. The transition has been observed in measurements of the decay of $^{204\text{m}}\text{Pb}$ (66.9 m) [9-11] and of ^{204}Bi [9]. It is therefore identified as an M1 transition between the spin-4 level at 1.5628 MeV and the 4^+ level at 1.2739 MeV.

Transition 2: 0.3307 MeV

This gamma ray is seen at several neutron bombarding energies in the present work and the threshold is <2 MeV, the cross section is ~ 0.1 b which is consistent with the strength measured for several other transitions excited in this experiment. However, on the basis of energetics, it does not fit into

the adopted level scheme for ^{204}Pb . The available information is too limited to permit identification of a new level.

Transition 3: 0.3618 MeV

This gamma ray is observed only at the highest bombarding energies of the present experiment ($E_n \sim 3$ MeV). This might be a transition between the 3^- level at 2.634 MeV and a level which is believed to exist in the vicinity of 2.268 MeV. Both of these levels have been observed in inelastic deuteron scattering [45]. However, because of the uncertainty in the excitation energies of these levels and the limited data available from the present experiment, this assignment is speculative.

Transition 4: 0.3750 MeV

This gamma ray is excited at neutron energies $\lesssim 2$ MeV and is clearly identified as an E2 transition between the 4^+ level at 1.2739 MeV and the 2^+ level at 0.89915 MeV. This same transition is observed strongly in the decay of $^{204\text{m}}\text{Pb}$ [9-11] and of ^{204}Bi [9]. The measured gamma-ray production cross section appears to exceed 0.1b above 2 MeV. Actually, the measured cross section is far smaller than the actual excitation strength because the 1.2739-MeV 4^+ level has a half life of ~ 0.29 μsec whereas the present experiment was designed to detect promptly emitted gamma rays. Based on the information in Section III.B, it is estimated that only $\sim 10\%$ of the transition strength was observed in the present experiment. Consequently, the actual excitation cross section for this transition is probably $\gtrsim 1$ b well above threshold.

Transition 5: 0.4518 MeV

The threshold for excitation of this gamma ray is < 2 MeV and the cross section is ~ 0.1 b well above the threshold region. There is no evidence for this transition in the decay of $^{204\text{m}}\text{Pb}$ [9-11] or of ^{204}Bi . However, there is

evidence for a level at 1.353 MeV from inelastic deuteron scattering measurements [45]. It seems very likely that this gamma ray comes from a transition between this 1.353-MeV level and the 2^+ level at 0.89915 MeV.

Transition 6: 0.6841 MeV

This gamma-ray is produced with a cross section of $\sim 0.2-0.3$ b well above threshold, and the threshold is below 2 MeV. The same transition has been observed in the $^{205}\text{Tl}(p,2n\gamma)^{204}\text{Pb}$ reaction and it is almost certainly an E2 transition between the 0^+ level at 1.584 MeV and the 2^+ level at 0.89915 MeV.

Transition 7: 0.7059 MeV

This gamma ray is seen at several energies and the threshold is <1.7 MeV. The cross section is >0.1 b well above threshold. However, it does not fit into the adopted level scheme for ^{204}Pb [9].

Transition 8: 0.766 MeV

The threshold for production of this gamma ray is <2 MeV. A spin-4 level at 1.663 MeV has been observed in the $^{206}\text{Pb}(p,t)^{204}\text{Pb}$ reaction. This gamma ray is probably an E2 transition between this level and the 2^+ level at 0.89915 MeV.

Transition 9: 0.7822 MeV

This gamma ray has a relatively low threshold (<2 MeV), and is excited with moderate strength (~ 0.1 b well above threshold). However, it does not fit into the adopted level scheme for ^{204}Pb [9].

Transition 10: 0.8618 MeV

This transition has a high threshold (near 3 MeV) and no cross sections were obtained. However, the gamma ray was observed in a long irradiation performed at $E_n \sim 3$ MeV. This might be an E1 transition between the 5^- level at 2.9285 MeV and the 5^+ level at 2.0649 MeV. It has not been observed in ^{204}Bi decay [9].

Transition 11: 0.8994 MeV

This gamma ray results from the decay of the 2^+ first-excited level at 0.89915 MeV. The cross section for production of this gamma ray is large and increases steadily with neutron energy since it is fed by an increasing number of transitions from higher-excited levels. Below ~ 1.3 MeV, the measured gamma-ray production cross section (Table 10 and Fig. 10) is nearly identical to the neutron inelastic scattering cross section for the 0.89915-MeV level. This cross section is ~ 0.5 - 0.6 b at ~ 1.3 MeV which is consistent with corresponding values computed for ^{206}Pb and ^{208}Pb by Fu and Perey [2]. The angular distributions for this gamma ray (Fig. 12, Tables 11 and 12) are typical of 2^+ (E2) 0^+ transitions.

Transition 12: 0.9187 MeV

This gamma ray is excited with a cross section of >0.1 b above 2 MeV. The gamma ray has also been seen in the decay of ^{204}Bi [9], and is identified as an E2 transition between the 4^+ level at 1.8174 MeV and the 2^+ level at 0.89915 MeV.

Transition 13: 0.9839 MeV

The cross section for this gamma ray is relatively large (~ 0.2 b at 3 MeV) and the threshold appears to be above 2 MeV. It is very likely that this is an E1 transition between the 5^- level at 2.2578 MeV and the 4^+ level at 1.2739 MeV. This transition is also observed in ^{204}Bi decay [9].

Transition 14: 1.0493 MeV

This transition has a high threshold and no cross sections were obtained. However, the gamma ray was observed in a long irradiation performed at $E_n \sim 3$ MeV. Based on energetics, this was first considered to be a transition between the 3^- level at 2.634 MeV and the 0^+ level at 1.584 MeV in which case the transition would be E3. However, E3 transitions are unfavored relative to

lower multiplicity transitions, which are possible to other levels below 2.634, so this assignment seemed very unlikely. We concluded that this gamma ray does not fit into the adopted level scheme [9].

Transition 15: 1.0617 MeV

A single cross section value of ~ 0.1 b at $E_n \sim 3$ MeV was obtained for this gamma ray. This gamma ray could be an E2 transition between the 2^+ level at 2.642 MeV and the 0^+ level at 1.584 MeV.

Transition 16: 1.2588 MeV

This gamma-ray line was observed very weakly at $E_n \sim 3$ MeV, and no cross sections were obtained. On the basis of energetics, this could be a transition between a level at 2.9.95 MeV and the 4^+ level at 1.663 MeV.

Transition 17: 1.2760 MeV

Evidence from the present experiment supports an assignment of 2^+ for the 1.353-MeV level. The 1.2760-MeV gamma ray was seen only at $E_n \sim 3$ MeV and no cross sections are available. This might be a transition between the 3^- level at 2.634 MeV and the 1.353-MeV level.

Transition 18: 1.3514 MeV

This is a strong gamma ray transition and clearly an E2 from the 1.353 MeV level to the 0^+ ground state.

Transitions 19-24: 1.5017, 1.663, 1.6820, 1.7223, 1.7619, and 1.8732 MeV

These gamma rays are excited only at the higher neutron energies of this experiment. A few scattered cross section values were obtained in the present work. For various reasons, it was not possible to fit any of these transitions into the adopted level scheme [9].

Transition 25: 1.9341 MeV

This gamma ray is probably the ground state E2 transition from the 2^+ level at 1.932 MeV. It has not been observed in other reaction studies on ^{204}Pb [9].

Clearly, there is considerable uncertainty in several of the assignments made above. The problem lies in the low sensitivity of the measurements. It was not possible to trace the excitation functions for most of the gamma rays to clearly defined thresholds.

IV. SURVEY OF AVAILABLE FAST-NEUTRON CROSS SECTION DATA FOR LEAD-204

The objective of this section is to provide the reader with an idea of the current status of the fast-neutron data base for ^{204}Pb . No attempt was made to compile these data or to evaluate the cross sections for significant reactions. We started our investigation by requesting the CSISRS File of Experimental Neutron Cross Sections for ^{204}Pb from the National Nuclear Data Center [5]. This file, in conjunction with CINDA-76/77 [4], was the basis for the survey. A compilation of plots of experimental cross sections from the National Nuclear Data Center [46] was also useful but it contained no information which was not already available from the CSISRS File [5].

A. Neutron Total and Elastic Scattering Cross Sections

A review of neutron nuclear data for ^{204}Pb should start with these important quantities since all partial cross sections must sum to the total cross section, and elastic scattering is a dominant interaction process at energies of interest for most applications. Unfortunately, in the case of ^{204}Pb , practically no data exist for the fast-neutron domain ($E_n > 0.1$ MeV).

Only one total cross section has been reported. This is the 14.2-MeV point of Dukarevich et al. [47]. Their value of 5.43 ± 0.06 b is consistent with the known magnitude for the cross section of elemental lead and for ^{208}Pb in this energy region [46]. There have been some measurements of the total cross section performed at the Linac facility ORELA at Oak Ridge National Laboratory in the resonance region ($E_n \lesssim 0.4$ MeV) by Good et al. [48] but none of these data have been published.

The situation for elastic scattering is worse since there are no reported measurements. This is unfortunate since it is not possible to generate a reliable optical model without accurate elastic scattering and total cross section data. Without such a model, computations of nonelastic cross sections are not reliable.

B. Neutron Inelastic Scattering

The only available data on inelastic scattering involves excitation of the 66.9-m isomer. This subject is discussed in Section II.

C. Neutron Capture

Measurements have been reported from Oak Ridge National Laboratory [49,50] and Rensselaer Polytechnic Institute [51]. Most of the available data have been measured using white-spectrum neutron sources and liquid scintillator detectors. The measurements of Macklin and Gibbons [49] employed monoenergetic neutrons.

Experimental data from these studies have been reported as resonance parameters and not cross sections, and they define the capture cross section from the keV region up to ~ 0.6 MeV. No cross sections are available for higher energies, however it should be possible to extrapolate to higher energies by means of theoretical calculations.

D. The (n;2n) Reaction

This reaction can be studied readily by the activation method since ^{203}Pb has only short-lived isomeric states ($t_{1/2} \leq 6$ sec) and the ground state decays with a 52.1 h half life to levels in ^{203}Tl and produces a gamma-ray spectrum which is amenable to activation measurements [52]. Considerable monoenergetic data are available which define the cross section from threshold at 8.44 MeV to ~ 20 MeV [28-31, 46, 53-61]. The available data have been analyzed by Davey et al. [62] in a study of the systematics of (n;2n) reactions. These authors obtained a reasonably good fit to the experimental data below the (n;3n) threshold at 15.3 MeV using a constant temperature nuclear model.

E. Other Neutron Reactions

There are no monoenergetic data available for the (n;3n) reaction. Based on systematics, the cross section is probably several hundred millibarns at

20 MeV. Some experimental data from fast reactor measurements have been reported for the (n;p) reaction [63,64]. No monoenergetic data are available, but the cross sections are probably $>10 \mu\text{b}$ well above threshold based on a measured spectrum average of $\sim 11 \mu\text{b}$.

V. SUMMARY

The cross section measurements performed in the present experiment have provided data on the $^{204}\text{Pb}(n;n')^{204\text{m}}\text{Pb}$ reaction which satisfy an existing request for these data [6] from threshold to ~ 10 MeV. Using these data and other available data for the 13-18 MeV range, an excitation function has been generated for this reaction which is consistent with available integral data to within the experimental errors.

The present work on the $^{204}\text{Pb}(n;n'\gamma)^{204}\text{Pb}$ prompt gamma rays indicates that this is a fruitful technique for nuclear structure studies of this nucleus. Greater sensitivity is clearly required.

The fast-neutron cross-section data base for ^{204}Pb is very limited. There is fairly detailed information available on capture, the $(n;2n)$ reaction and excitation of the 66.9-m isomer. There are practically no total or elastic scattering cross section data available. This is a serious defect since it is not possible to develop a reliable optical model for computational purposes without these experimental quantities to constrain the model parameters.

APPENDIX A

NEUTRON SCATTERING CALCULATIONS FOR
COAXIAL CYLINDER GEOMETRIES

Neutron scattering corrections for the ^{204}mPb activation measurements were computed using the techniques described in this Appendix, as incorporated into Monte Carlo program CYSCAT, which has been developed by one of the authors (JWM). The applications for this code are more general than the current experiment; however, the procedures have not been documented previously.

The program CYSCAT is designed to calculate neutron scattering into detectors for systems having cylindrical geometry. It permits the inclusion of source angular and energy distributions as well as energy-dependent cross sections and angular-distribution coefficients. However, it only considers single scattering and its use should be restricted to those situations where the transmission through scatterer and detector is large. The original purpose of this program was to calculate scattering from lightly-constructed source and detector structures. In these cases most multiple-scattering events involve long neutron flight paths and are often eliminated by fast-timing techniques.

The basic geometry of the system is shown in Fig. 13. The neutron source is some neutron producing reaction such as $^7\text{Li}(p;n)^7\text{Be}$ or $\text{D}(d;n)\text{T}$ and occupies a line of length l_n as shown. The scatterer is a ring or disk and may be located anywhere as long as its axis coincides with the source axis. The detector is a cylinder, always located to the right of the source. The scatterer and the detector may be identical.

All cross sections associated with the scatterer and the detector, and the ω coefficients for the scattering angular distribution are entered as interpolation tables. Interpolation is linear. The ω coefficients for the neutron-source reaction are entered with the incident partial energy of the particular problem. All angular distributions are expressed as

$$F(\theta) = 1 + \sum_{i=1}^n \omega_i P_i(\cos \theta) \quad (\text{A.1})$$

where $P_i(\cos \theta)$ is the appropriate Legendre function.

The angular distributions are given in the center of mass system but angles are chosen in the laboratory system. The center of mass angle, θ , is calculated by subroutine LABEGY. The angular distribution in the laboratory system for A_3 is

$$F(\theta_0) = F(\theta)C(\theta) \quad (\text{A.2})$$

$$C(\theta) = \frac{(1 + \gamma^2 + 2\gamma \cos \theta)^{3/2}}{|1 + \gamma \cos \theta|} \quad (\text{A.3})$$

$$\gamma = \left[\frac{A_1 A_3 (E_{p1} - E_{cm})}{A_2 A_4 (E_{p1} - E_{cm} + Q)} \right]^{1/2} \quad (\text{A.4})$$

where

$$\left. \begin{array}{l} A_1 \\ A_2 \\ A_3 \\ A_4 \end{array} \right\} = \text{reactant and product masses}$$

E_{cm} = energy associated with the center of mass motion

Q = energy associated with the reaction

E_{p1} = laboratory energy of A_1 .

Subroutine LABEGY also provides the laboratory energy for the neutron E_1 . Under some conditions there are two values for this energy. In this case the subroutine provides both energies and center-of-mass angles and a random choice is made based on the relative values $F(\theta_0)$ for θ_1 and θ_2 .

The source is divided into ten layers of equal thickness and equal numbers of neutrons are produced in each layer. The effective energy of the incident particle for producing a reaction in the j^{th} layer is

$$E_{pj} = E_{pi} - (j - \frac{1}{2}) \left(\frac{dE}{dt} \right) \frac{\lambda_n}{10} \quad (\text{A.5})$$

where

E_{pi} = the incident energy

λ_n = source thickness

(dE/dt) = rate of energy loss in the source.

The neutron direction, $\cos \theta_0$, in the laboratory system, is chosen at random within the limits set by the system geometry as illustrated in Fig. 13;

$$\cos \theta_0 = \cos \theta_{0\min} - N_r (\cos \theta_{0\min} - \cos \theta_{0\max}), \quad (\text{A.6})$$

where N_r is a random number between 0 and 1.

The source strength for a single neutron is given by

$$S(\theta_0) = F(\theta_0) (\cos \theta_{0\min} - \cos \theta_{0\max}) / 2 \quad (\text{A.7})$$

The neutron path length through the scatterer, L , is calculated by subroutine PATHL. The scattering location is chosen by making a random choice

$$T_z = -\lambda_n [1 - N_r (1 - e^{-L_{si} N_s \sigma_{tsi}})] \cos \theta_0 / (N \sigma_{tsi}) \quad (\text{A.8})$$

where

T_z = depth of penetration into the scatterer parallel to the axis.

N_r = random number

σ_{tsi} = scatterer total cross section at neutron energy E_1

N_s = scatterer atoms/cm³

L_{si} = maximum path length in scatterer.

At this point the laboratory scattering angles, θ_s and ϕ are chosen. In order to improve the program efficiency in circumstances where the detector solid angle (as seen from the scatterer) is small, limits may be set on $\cos \theta_s$ and on ϕ . This feature is an option that may be exercised at run time. The scattering probability is

$$P_s(\theta_s, \phi, E) = \frac{F(\theta_s)(\cos \theta_{smin} - \cos \theta_{smax})(\phi_{max} - \phi_{min})}{2} \cdot T_d(E_1, \theta_s, \phi) \cdot (1 - e^{-L_{s1} N_s \sigma_{ts1}}) \frac{\sigma_{s1}}{\sigma_{ts1}} \quad (A.9)$$

$F(\theta_s)$ = similar to $F(\theta)$ in Eq. (2)

T_d = transmission through detector if it is between source and scatterer

σ_{s1} = scattering cross section for scatterer at energy E_1 .

The path lengths of the scattered neutron in the scatterer L_{s2} , and the detector, L_{d2} , are calculated by PATHL. If L_{d2} is zero, calculations on this history are terminated. Otherwise the energy of the scattered particle, E_2 , is obtained from LABEGY. The Q of the scattering reaction is zero for elastic scattering or is some fixed value for scattering to a specific level. For general inelastic scattering the Q is chosen at random weighted by a simple temperature distribution of the form

$$F(Q) \propto (E_{max} + Q)e^{-Q/T} \quad (A.10)$$

$$Q = E - E_{max}$$

E_{max} = the maximum energy of an evaporated neutron

E = center of mass energy of evaporated neutron.

The probability of detecting a scattered neutron is

$$P_d(E_2) = e^{-L_{s2} N_s \sigma_{ts2}} (1 - e^{-L_{d2} N_d \sigma_{td2}}) \frac{\sigma_{rd2}}{\sigma_{td2}} \quad (A.11)$$

σ_{td2} = detector total cross section at energy E_2

σ_{rd2} = detector reaction cross section at energy E_2 .

The probability of a source neutron being scattered and detailed in

$$G_s = S(\theta_0) P(\theta_s, \phi, E_1) P_d(E_2). \quad (A.12)$$

The probability of detecting a neutron directly from the source is obtained in a similar fashion except the choice of the angle θ_{od} is made within limits imposed by the detector dimensions.

$$G_d = S(\theta_{od}) \{ e^{-L_s N_s \sigma_{ts}} (1 - e^{-L_d N_d \sigma_{td}}) \frac{\sigma_{rd}}{\sigma_{td}} \quad (A.13)$$

The term within { } is the transmission through the scatterer when it is between the source and detector.

The fractional standard deviation is obtained from the variance of the calculation

$$\Delta_s = \left(\frac{\langle G_s^2 \rangle - \langle G_s \rangle^2}{\langle G_s \rangle^2} \right)^{1/2} \quad (A.14)$$

The error in the ratio (D_s/D_d) is

$$\Delta R = (\Delta_s^2 + \Delta_d^2)^{1/2}. \quad (A.15)$$

Subroutine LABEGY

This is a simple non-relativistic kinematic calculation for the reaction

$$A_1 + A_2 = A_3 + A_4 + Q.$$

The input is the reactant and product masses, Q , the laboratory energy of A_1 and the laboratory angle of A_3 .

The output is the laboratory energy of A_3 and its center of mass angle.

In those cases where two kinematic groups are possible, both laboratory energies and center-of-mass angles are provided.

Subroutine PATHL

This is a subroutine for calculating the path length of a vector through a cylinder of length T and radius R located at a distance z_m from the origin.

The origin of the vector is at $z = 0$ and radius R_v . The subroutine is entered with this information plus the vector direction cosines l , m , and n .

The two points of interaction of a cylinder of radius R and of infinite length are calculated

$$z_{1,2} = \frac{-R_v l \pm [R^2(l^2 + m^2) - R_v^2 m^2]^{1/2}}{l^2 + m^2}$$

If z_1 and z_2 are imaginary

$$L_p = 0 \text{ exit}$$

If $z_1 < z_m$ and $z_2 < z_m$

$$L_p = 0 \text{ exit}$$

If $z_1 > (z_m + T)$ and $z_2 > (z_m + T)$

$$L_p = 0 \text{ exit}$$

If $z_1 > z_m$ and $z_1 < (z_m + T)$

$$L_1 = z_1/n$$

If $z_2 < (z_m + T)$ and $z_2 > z_m$

$$L_2 = z_2/n$$

If $z_1 < z_m$

$$L_1 = z_m/n$$

If $z_2 > (z_m + T)$

$$L_2 = (z_m + T)/n$$

If L_1 or L_2 is negative it is set equal to zero and

$$L_p = |L_2 - L_1|.$$

REFERENCES

1. "Chart of the Nuclides," prepared by Norman E. Holden and William Walker, Knolls Atomic Power Laboratory, General Electric Company, Schenectady, N. Y. 12345 (1972).
2. C. Y. Fu and F. G. Perey, "An Evaluation of Neutron and Gamma-Ray-Production Cross-Section Data for Lead," Atomic Data and Nuclear Data Tables 16, 409 (1975).
3. "Evaluated Neutron Data File, ENDF/B-IV," National Neutron Cross Section Center, Brookhaven National Laboratory, Upton, N. Y. 11973, U.S.A. (1975).
4. "CINDA-76/77, An Index to the Literature on Microscopic Neutron Data," International Atomic Energy Agency, Vienna (1976). Includes Supls. 1 and 2.
5. "Experimental Data File, CSISRS," National Neutron Cross Section Center, Brookhaven National Laboratory, Upton, N. Y. 11973, U.S.A. (1977).
6. "Compilation of Requests for Nuclear Data," compiled and edited by Leona Stewart, Michael S. Moore and Henry T. Motz, LA-5253-MS, Los Alamos Scientific Laboratory (1973).
7. C. M. Ko, T. T. S. Kuo and J. B. McGrony, Phys. Rev. C8, 2379 (1973).
8. J. B. McGroory and T. T. S. Kuo, Nucl. Phys. A247, 283 (1975).
9. "Nuclear Data Sheets for A = 204," M. J. Martin, Nucl. Data B5, 601 (1971).
10. A. Hansen, Z. Physik 245, 204 (1971).
11. Jean Guile, R. E. Doebler, Wm. C. McHarris and W. H. Kelly, Phys. Rev. C5, 2107 (1972).
12. C. Signorini and H. Moninaga, Physics Letters 408, 549 (1972).
13. Stable Isotopes Division, Oak Ridge National Laboratory, Oak Ridge, Tennessee, U.S.A.
14. Donald L. Smith, "A Spectrometer for the Investigation of Gamma Radiation Produced by Neutron-Induced Reactions," ANL/NDM-12, Argonne National Laboratory (1973).
15. S. Elbaker, I. van Heerden, W. Dawson, W. McDonald and G. Nielson, Nucl. Instr. and Meth. 97, 283 (1971).
16. J. W. Meadows and D. L. Smith, "Neutrons from Proton Bombardment of Natural Lithium," ANL-7938, Argonne National Laboratory (1972).
17. Donald L. Smith and James W. Meadows, "Measurement of $^{58}\text{Ni}(n;p)^{58}\text{Co}$ Reaction Cross Sections for $E_n = 0.44-5.87$ MeV Using Activation Methods," ANL-7989, Argonne National Laboratory (1973).
18. D. L. Smith and J. W. Meadows, "Method of Neutron Cross Section Measurement for $E_n = 5.5-10$ MeV Using the $D(d,n)$ He-3 Reaction as a Neutron Source," ANL/NDM-9, Argonne National Laboratory (1974).
19. Donald L. Smith and James W. Meadows, "Cross Sections for the $^{66}\text{Zn}(n;p)^{66}\text{Cu}$, $^{113}\text{In}(n;n')^{113\text{m}}\text{In}$ and $^{115}\text{In}(n;n')^{115\text{m}}\text{In}$ Reactions from Near Threshold to 10 MeV," ANL/NDM-14, Argonne National Laboratory (1975).

20. R. W. Lamphere, "Fission Detectors," in Fast Neutron Physics I, eds. J. B. Marion and J. L. Fowler, Interscience, New York, 721 (1960).
21. Donald L. Smith and James W. Meadows, "Cross Sections for (n;p) Reactions on ^{27}Al , $^{46,47,48}\text{Ti}$, $^{54,56}\text{Fe}$, ^{58}Ni , ^{59}Co and ^{64}Zn from Near Threshold to 10 MeV," ANL/NDM-10, Argonne National Laboratory (1975).
22. Donald L. Smith and James W. Meadows, "Response of Several Threshold Reactions in Reference Fission Neutron Fields," ANL/NDM-13 (1975).
23. A. C. G. Mitchell, "The Coincidence Method," in Beta- and Gamma-Ray Spectroscopy, ed. Kai Siegbahn, Interscience (1955).
24. A. J. Ferguson, Angular Correlation Methods in Gamma-Ray Spectroscopy, Interscience (1965).
25. "Evaluated Neutron Data File, ENDF/B-IV," National Nuclear Data Center, Brookhaven National Laboratory.
26. E. Storm and H. I. Israel, "Photon Cross Sections from 1 keV to 100 MeV for Elements $Z = 1$ to $Z = 100$," Nuclear Data Tables A7, 565 (1970).
27. H. Liskien and A. Paulsen, Nucl. Data 11, 569 (1973).
28. A. K. Hankla, R. W. Fink and J. H. Hamilton, Nucl. Phys. A180, 157 (1972).
29. J. Csikai and G. Peto, Acta Phys. Hung. 23, 87 (1967).
30. P. Decowski, W. Grochulski, A. Marcinkowski, J. Karolyi, J. Piotrowski, E. Saad, K. Siwek-Wilczynska and I. M. Turkiewicz, Nucl. Phys. A204, 121 (1973).
31. G. N. Maslov, F. Nasyrov and N. F. Pashkin, Report YK-9, 50, Obninsk Reports, Soviet Union (1972).
32. A. Calamand, in Handbook on Nuclear Activation Cross Sections, Technical Report Series No. 156, International Atomic Energy Agency, Vienna (1974) p. 273.
33. R. W. Durham, M. P. Navalkar and E. Ricci, Report, AECL-1434, Chalk River Nuclear Laboratories, Canada (1962).
34. W. Koehler, Nukleonik 10, 181 (1967).
35. I. Kimura, K. Kobayashi and T. Shibata, J. Nucl. Sci. Technology (Tokyo) 8, 59 (1971).
36. "ENDF/B-IV Dosimetry File," ed. B. A. Magurno, BNL-NCS-50446, Brookhaven National Laboratory (1975).
37. Donald L. Smith, "Analysis of the Sensitivity of Spectrum-Average Cross Sections to Individual Characteristics of Differential Excitation Functions," ANL/NDM-30, Argonne National Laboratory (1977).
38. Donald L. Smith, "A Spectrometer for the Investigation of Gamma Radiation Produced in Neutron-Induced Reactions," ANL/NDM-12, Argonne National Laboratory (1975).
39. Donald L. Smith, "Sample-Size Effects in Fast-Neutron Gamma-Ray Production Measurements: Solid-Cylinder Samples," ANL/NDM-17 (1975).
40. Donald L. Smith, "Fast-Neutron Gamma-Ray Production from Elemental Iron: $E_n \sim 2$ MeV," ANL/NDM-20 (1976).

41. W. P. Poenitz and J. F. Whalen, "On-Line Computer Facility and Operating System COSACS at the ANL Fast Neutron Generator," ANL-8026, Argonne National Laboratory (1973).
42. R. B. Day, Phys. Rev. 102, 767 (1965); Progress in Fast Neutron Physics, ed. G. C. Phillips, J. B. Marion and J. R. Riser, Univ. of Chicago Press (1963).
43. E. Sheldon and D. M. Van Patter, Rev. Mod. Phys. 38, 143 (1966).
44. W. E. Kinney and F. G. Perey, Nucl. Sci. Eng. 63, 418 (1977).
45. J. H. Bjerregaard, O. Hansen, O. Nathan and S. Hinds, Nucl. Phys. A94, 457 (1967).
46. D. I. Garber and R. R. Kinsey, "Neutron Cross Sections, Vol. II-Curves," BNL-325, Third Edition, Vol. 2, National Nuclear Data Center, Brookhaven National Laboratory (1976).
47. Yu. V. Dukarevich, A. N. Dyumin and D. M. Kaminker, Nucl. Phys. A92, 433 (1967).
48. W. Good et al., USNDC-7, p. 172 (1973).
49. R. Macklin and J. Gibbons, Phys. Rev. 159, 1007 (1967).
50. B. J. Allen, R. L. Macklin, R. R. Winters and C. Y. Fu, Phys. Rev. C8, 1504 (1973).
51. R. H. Wolfe, Z. M. Bartolome, J. R. Tatarczuk, R. W. Hockenbury and R. C. Block, WASH-1127, p. 173 (1969).
52. Nuclear Level Schemes A = 45 through A = 257 from Nuclear Data Sheets, ed. Nuclear Data Group, Oak Ridge National Laboratory, Academic Press (1973).
53. H. A. Tewes, A. A. Caretto, A. E. Miller and D. R. Nethaway, "Excitation Functions of Neutron-Induced Reactions," UCRL-6028-T, Lawrence Livermore Laboratory (1960).
54. M. Borman, C. Abels, W. Carstens and I. Richle, EANDC(E)-76, p. 51 (1967).
55. F. J. Vaughn, Priv. Communication to National Nuclear Data Center (1963).
56. W. Dilg, H. Vonach, G. Winkler and P. Hille, Nucl. Phys. A118, 9 (1968).
57. J. Karolyi et al., Nucl. Phys. A122, 234 (1968).
58. G. Winkler, Oesterr. Akad. Wiss., Math. Naturw., Sitzber 177, 323 (1969).
59. J. Janczyszyn and L. Gorski, J. Radio and Chem. 14, 201 (1973).
60. E. Ruranz, J. Chwaszezewska, Z. Haratym, M. Pietrzykowski and A. Sulik, Acta Phys. Polonica B2, 553 (1971).
61. J. Araminowicz and J. Dresler, INR-1464, p. 14, Inst. Badan Jadrowych, Warsaw (1973).
62. W. G. Davey, R. W. Goin and J. R. Ross, "An Analysis of (n;2n) Cross-Section Measurements for Nuclei up to Mass 238," ANL-75-34, Argonne National Laboratory (1975).
63. J. C. Roy, CRC-1003, Chalk River Laboratories, Canada (1960).
64. J. Op de Beeck, A. Speecke and J. Hoste, Radiochimica Acta 4, 32 (1965).

TABLE 1. Specifications for the ^{204}Pb -Enriched Sample^a

Mass: 9.569 g metal

Geometry: Cylinder, 2.544 cm dia x 0.17 cm thick

Isotopic Abundances

| Isotope | Atomic Percent | Precision |
|---------|----------------|-----------|
| 204 | 99.73 | ±0.02 |
| 206 | 0.17 | ±0.01 |
| 207 | 0.05 | ±0.01 |
| 208 | 0.06 | ±0.01 |

Chemical Impurities Content

| Element | Atomic Percent | Element | Atomic Percent |
|---------|----------------|---------|----------------|
| Ag | <0.01T | Mg | <0.01 |
| Al | <0.05 | Mn | <0.02 |
| B | <0.01 | Mo | <0.02 |
| Ba | <0.01 | Na | <0.01 |
| Be | <0.001 | Ni | <0.05 |
| Bi | <0.02 | Pt | <0.05 |
| C | <0.05 | Rb | <0.02 |
| Ca | <0.01 | Sb | <0.05 |
| Cd | <0.05 | Si | <0.01 |
| Co | <0.05 | Sn | <0.02 |
| Cr | <0.05 | Sr | <0.01 |
| Cs | <0.05 | Ta | <0.05 |
| Cu | <0.01 | Ti | <0.01 |
| Fe | <0.02 | V | <0.02 |
| Ge | <0.05 | W | <0.05 |
| Hg | <0.05 | Zn | <0.2 |
| Li | <0.005 | Zr | <0.05 |

^aData obtained from the Stable Isotopes Division, Oak Ridge National Laboratory.

TABLE 2. Specifications for the Elemental Lead Samples^a

Mass: ~10.7 g

Geometry: Cylinders, 2.54 cm dia x 0.188 cm thick

Isotopic Abundances

| Isotope | Atomic Percent | Precision (1 σ) |
|---------|----------------|-------------------------|
| 204 | 1.35 | |
| 206 | 25.48 | ± 0.01 |
| 207 | 21.14 | ± 0.05 |
| 208 | 52.02 | ± 0.05 |
| | | ± 0.11 |

Chemical Impurities Content

| Element | Atomic Percent | Element | Atomic Percent |
|---------|----------------|---------|----------------|
| Ag | 0.03 | Li | <0.001 |
| Al | 0.004 | Mg | <0.01 |
| As | <0.1 | Mn | <0.001 |
| B | <0.01 | Mo | <0.01 |
| Ba | <0.01 | Na | <0.01 |
| Be | <0.001 | Ni | Trace |
| Bi | 0.07 | Sb | <0.01 |
| Ca | <0.1 | Si | <0.01 |
| Co | <0.01 | Sn | Faint trace |
| Cr | <0.01 | Ti | <0.01 |
| Cu | 0.2 | V | <0.01 |
| Fe | <0.01 | Zn | <0.2 |
| Hg | <0.1 | Zr | <0.1 |
| K | <0.01 | | |

^a Analysis performed in the Analytical Laboratory, Argonne National Laboratory.

TABLE 3. Specifications for Uranium Deposits Used as Neutron Fluence Monitors in the $^{204\text{m}}\text{Pb}$ Activation Measurements

| Deposit | Isotope Content (Number of Atoms) | | | |
|---------------------------|-----------------------------------|------------------------|------------------------|------------------------|
| | ^{234}U | ^{235}U | ^{236}U | ^{238}U |
| ^{235}U enriched | 2.78×10^{16} | 2.646×10^{18} | 1.223×10^{16} | 2.743×10^{15} |
| ^{238}U enriched | ~ 0 | ~ 0 | ~ 0 | 4.857×10^{18} |

TABLE 4. Neutron Scattering Corrections for the
 ^{204}Pb Activation Measurements^a

| E_n (MeV) | Alpha | Beta | Gamma | | Rho | |
|----------------|-------|------|------------------|------------------|------------------|------------------|
| | | | ^{235}U | ^{238}U | ^{235}U | ^{238}U |
| 0.165 | - | - | 5.54 | 5.14 | 3.89 | 2.87 |
| 0.291 | - | - | 4.88 | 4.58 | 7.14 | 6.0 |
| 0.406 | - | - | 3.99 | 3.6 | 5.49 | 4.09 |
| 0.572 | - | - | 2.85 | 2.73 | 4.42 | 3.18 |
| 0.786 | - | - | 3.15 | 2.94 | 3.64 | 2.5 |
| 0.995 | - | - | 2.92 | 2.89 | 3.36 | 2.03 |
| 1.202 | - | - | 2.96 | 2.88 | 3.49 | 1.78 |
| 1.408 | - | - | 4.09 | 2.85 | 3.74 | 1.57 |
| 1.612 | - | - | 4.07 | 3.08 | 3.51 | 1.61 |
| 1.816 | - | - | 4.29 | 3.24 | 3.83 | 2.06 |
| 2.019 | - | - | 4.28 | 3.38 | 4.38 | 2.78 |
| 2.525 | 2.99 | 0.08 | 4.52 | 3.51 | 5.13 | 3.82 |
| 3.029 | 3.88 | 0.68 | 4.81 | 3.93 | 4.55 | 3.13 |
| 3.532 | 3.39 | 0.88 | 4.46 | 3.83 | 4.51 | 3.17 |
| 4.035 | 3.0 | 1.13 | 4.71 | 3.75 | 5.1 | 3.49 |
| 4.336 | 2.73 | 1.1 | 4.48 | 3.51 | 4.77 | 3.42 |
| 4.637 | 2.44 | 1.11 | 4.56 | 3.43 | 4.73 | 3.47 |
| 5.0 | 2.18 | 1.34 | 4.59 | 3.29 | 4.81 | 3.53 |
| 5.2 | 2.08 | 1.03 | 4.53 | 3.36 | 4.72 | 3.38 |
| 5.6 | 1.96 | 1.47 | 4.22 | 3.15 | 4.46 | 3.15 |
| 6.265 | 1.9 | 1.02 | 3.87 | 2.73 | 3.62 | 2.43 |
| 7.261 | 1.49 | 0.74 | 3.1 | 2.35 | 2.67 | 1.89 |
| 8.239 | 1.49 | 0.9 | 2.92 | 2.19 | 2.8 | 2.03 |
| 9.207 | 1.51 | 0.87 | 2.71 | 2.21 | 2.48 | 1.98 |
| 10.17 | 1.3 | 0.92 | 2.29 | 2.0 | 2.46 | 1.8 |
| 11.12 | 1.27 | 0.77 | 2.15 | 1.85 | 2.2 | 1.72 |

^aValues given in percent.

TABLE 5. Sources of Experimental Error in the
 ^{204}Pb Activation Measurements

| Source of Error | Magnitude (%) |
|--|-------------------|
| 1. Error in detector counts | Variable |
| 2. Gamma-ray detector efficiency | 6 |
| 3. Decay half life effects | <1 |
| 4. Geometric considerations | 2 |
| 5. Neutron source properties | 2 |
| 6. Scattering corrections ^a | <1 |
| 7. Mass of uranium deposit | 1 |
| 8. Number of ^{204}Pb atoms in sample | (2%) ^b |
| 9. Miscellaneous errors | 1 |

^aNeutron scattering corrections largely cancel in the cross section calculations.

^bThis error is negligible for the ^{204}Pb -enriched sample.

TABLE 6. Measured Cross Section Ratios and Calculated Cross Sections for the $^{204}\text{Pb}(n;n')^{204\text{m}}\text{Pb}$ Reaction

| E_n (MeV) | Resolution (MeV) | Sample | Monitor | Neutron Source | Ratio ($\sigma_{mn'}/\sigma_f$) | Ratio Error (%) | σ_f^b (b) | $\sigma_{nn'}^b$ (b) |
|----------------|---------------------|-------------------|------------------|-------------------|--------------------------------------|--------------------|---------------------|-------------------------|
| 2.220 | 0.065 | ^{204}Pb | ^{235}U | Li^a | 1.646×10^{-5} | 55.4 | 1.276 | 2.100×10^{-5} |
| 2.348 | 0.061 | | ^{238}U | | 3.143×10^{-4} | 21.2 | 0.5488 | 1.725×10^{-4} |
| 2.390 | 0.065 | | ^{235}U | | 4.663×10^{-4} | 11.1 | 0.5486 | 2.558×10^{-4} |
| 2.424 | 0.068 | | ^{238}U | | 4.878×10^{-4} | 10.4 | 1.280 | 6.244×10^{-4} |
| 2.488 | 0.083 | | ^{235}U | | 3.833×10^{-3} | 7.7 | 0.5482 | 2.101×10^{-3} |
| 2.520 | 0.069 | | ^{238}U | | 3.473×10^{-3} | 7.4 | 1.280 | 4.446×10^{-3} |
| 2.585 | 0.097 | | ^{235}U | | 1.129×10^{-2} | 7.3 | 0.5478 | 6.187×10^{-3} |
| 2.619 | 0.071 | | ^{238}U | | 5.483×10^{-3} | 7.7 | 1.271 | 6.969×10^{-3} |
| 2.628 | 0.088 | | ^{235}U | | 1.236×10^{-2} | 7.3 | 0.5477 | 6.770×10^{-3} |
| 2.631 | 0.124 | El. Pb | ^{238}U | | 1.212×10^{-2} | 9.9 | 0.5477 | 6.639×10^{-3} |
| 2.690 | 0.125 | ^{204}Pb | | | 1.777×10^{-2} | 9.0 | 0.5474 | 9.730×10^{-3} |
| 2.736 | 0.089 | El. Pb | | | 1.785×10^{-2} | 7.2 | 0.5472 | 9.765×10^{-3} |
| 2.740 | 0.126 | | | | 2.092×10^{-2} | 8.6 | 0.5472 | 1.145×10^{-2} |
| 2.790 | 0.126 | | | | 2.389×10^{-2} | 8.3 | 0.5470 | 1.307×10^{-2} |
| 2.842 | 0.127 | | | | 2.434×10^{-2} | 9.0 | 0.5468 | 1.331×10^{-2} |
| 2.891 | 0.127 | | | | 3.242×10^{-2} | 8.0 | 0.5466 | 1.772×10^{-2} |
| 2.941 | 0.128 | | | | 2.881×10^{-2} | 9.0 | 0.5464 | 1.574×10^{-2} |
| 2.959 | 0.153 | ^{204}Pb | | | 4.140×10^{-2} | 7.0 | 0.5464 | 2.262×10^{-2} |
| 2.991 | 0.129 | El. Pb | | | 3.863×10^{-2} | 7.8 | 0.5462 | 2.110×10^{-2} |
| 3.041 | 0.129 | | | | 4.137×10^{-2} | 8.0 | 0.5460 | 2.259×10^{-2} |
| 3.091 | 0.130 | | | | 4.826×10^{-2} | 7.8 | 0.5458 | 2.634×10^{-2} |
| 3.141 | 0.131 | | | | 4.778×10^{-2} | 7.8 | 0.5456 | 2.607×10^{-2} |
| 3.203 | 0.108 | | | | 5.688×10^{-2} | 7.6 | 0.5454 | 3.102×10^{-2} |
| 3.241 | 0.132 | | | | 5.662×10^{-2} | 7.8 | 0.5452 | 3.087×10^{-2} |
| 3.291 | 0.133 | | | | 6.028×10^{-2} | 7.8 | 0.5450 | 3.285×10^{-2} |
| 3.345 | 0.111 | | | | 6.359×10^{-2} | 7.6 | 0.5466 | 3.476×10^{-2} |
| 3.368 | 0.114 | | ^{235}U | | 3.191×10^{-2} | 7.6 | 1.201 | 3.832×10^{-2} |
| 3.380 | 0.154 | | ^{238}U | | 6.627×10^{-2} | 7.6 | 0.5479 | 3.631×10^{-2} |
| 3.388 | 0.134 | | | | 6.501×10^{-2} | 7.6 | 0.5482 | 3.564×10^{-2} |
| 3.437 | 0.153 | ^{204}Pb | | | 6.736×10^{-2} | 7.6 | 0.5499 | 3.704×10^{-2} |
| 3.437 | 0.154 | El. Pb | | | 6.730×10^{-2} | 7.5 | 0.5499 | 3.701×10^{-2} |

TABLE 6 (Contd.)

| E_n (MeV) | Resolution (MeV) | Sample | Monitor | Neutron Source | Ratio ($\sigma_{nn'}/\sigma_f$) | Ratio Error (%) | σ_f^b (b) | $\sigma_{nn'}^b$ (b) | |
|----------------|---------------------|----------------------------------|------------------|--|--------------------------------------|------------------------|------------------------|-------------------------|------------------------|
| 3.468 | 0.115 | El. Pb ↓ ^{204}Pb | ^{235}U | Li^a ↓ D^c Li^a ↓ D^c | 3.400×10^{-2} | 7.6 | 1.192 | 4.053×10^{-2} | |
| 3.480 | 0.154 | | ^{238}U | | 6.902×10^{-2} | 7.9 | 0.5514 | 3.806×10^{-2} | |
| 3.573 | 0.116 | | ^{235}U | | 3.729×10^{-2} | 7.9 | 1.183 | 4.411×10^{-2} | |
| 3.585 | 0.154 | | ^{238}U | | 8.018×10^{-2} | 8.1 | 0.5541 | 4.443×10^{-2} | |
| 3.664 | 0.117 | | ^{235}U | | 4.232×10^{-2} | 7.8 | 1.175 | 4.973×10^{-2} | |
| 3.677 | 0.154 | | ^{238}U | | 8.519×10^{-2} | 7.5 | 0.5585 | 4.758×10^{-2} | |
| 3.763 | 0.118 | | ^{235}U | | 4.634×10^{-2} | 7.6 | 1.165 | 5.399×10^{-2} | |
| 3.778 | 0.154 | | ^{238}U | | 9.027×10^{-2} | 7.5 | 0.5621 | 5.074×10^{-2} | |
| 3.861 | 0.119 | | ^{235}U | | 4.920×10^{-2} | 7.7 | 1.156 | 5.688×10^{-2} | |
| 3.878 | 0.155 | | ^{238}U | | 9.547×10^{-2} | 7.5 | 0.5656 | 5.399×10^{-2} | |
| 3.955 | 0.150 | | ^{235}U | | 4.731×10^{-2} | 7.4 | 1.147 | 5.426×10^{-2} | |
| 3.960 | 0.120 | | | | ^{235}U | 5.324×10^{-2} | 7.8 | 1.147 | 6.107×10^{-2} |
| 3.979 | 0.155 | | | | ^{238}U | 0.1069 | 7.5 | 0.5693 | 6.088×10^{-2} |
| 3.998 | 0.143 | | | 0.1068 | 7.5 | 0.5700 | 6.087×10^{-2} | | |
| 4.062 | 0.155 | ^{204}Pb | | 0.1118 | 7.0 | 0.5693 | 6.363×10^{-2} | | |
| 4.097 | 0.145 | El. Pb | | 0.1146 | 7.6 | 0.5688 | 6.520×10^{-2} | | |
| 4.198 | 0.146 | | | 0.1198 | 7.6 | 0.5676 | 6.802×10^{-2} | | |
| 4.298 | 0.148 | | | 0.1260 | 7.6 | 0.5664 | 7.134×10^{-2} | | |
| 4.404 | 0.150 | | | 0.1327 | 7.6 | 0.5652 | 7.499×10^{-2} | | |
| 4.503 | 0.151 | | | 0.1405 | 7.7 | 0.5640 | 7.922×10^{-2} | | |
| 4.603 | 0.153 | | | 0.1430 | 7.5 | 0.5628 | 8.048×10^{-2} | | |
| 4.703 | 0.154 | | | 0.1578 | 7.7 | 0.5616 | 8.861×10^{-2} | | |
| 4.804 | 0.156 | | | 0.1664 | 7.6 | 0.5604 | 9.323×10^{-2} | | |
| 4.903 | 0.157 | ^{204}Pb | | 0.1648 | 7.0 | 0.5592 | 9.216×10^{-2} | | |
| 4.903 | 0.158 | El. Pb | | 0.1643 | 7.7 | 0.5592 | 9.187×10^{-2} | | |
| 5.004 | 0.159 | | | 0.1718 | 7.7 | 0.5580 | 9.589×10^{-2} | | |
| 5.103 | 0.161 | | | 0.1587 | 7.9 | 0.5568 | 8.835×10^{-2} | | |
| 5.105 | 0.309 | | | 0.1834 | 7.6 | 0.5567 | 0.1021 | | |
| 5.201 | 0.163 | | | 0.1727 | 7.8 | 0.5556 | 9.593×10^{-2} | | |
| 5.301 | 0.164 | | | 0.1877 | 7.8 | 0.5577 | 0.1047 | | |
| 5.456 | 0.291 | | | 0.1941 | 7.6 | 0.5663 | 0.1099 | | |
| 5.867 | 0.278 | | | 0.2005 | 7.5 | 0.6223 | 0.1248 | | |

TABLE 6 (Contd.)

| E_n (MeV) | Resolution (MeV) | Sample | Monitor | Neutron Source | Ratio ($\sigma_{nn'}/\sigma_f$) | Ratio Error (%) | σ_f^b (b) | $\sigma_{nn'}$ (b) |
|----------------|---------------------|-------------|-----------------------|-------------------|--------------------------------------|--------------------|---------------------|-----------------------|
| 6.414 | 0.270 | El. Pb ↓ | ^{238}U ↓ | D^c ↓ | 0.1888 | 7.7 | 0.8060 | 0.1522 |
| 6.424 | 0.331 | | | | 0.1821 | 8.0 | 0.8094 | 0.1474 |
| 6.934 | 0.269 | | | | 0.2103 | 7.7 | 0.8128 | 0.1709 |
| 7.443 | 0.273 | | | | 0.1992 | 7.5 | 0.9676 | 0.1927 |
| 7.945 | 0.279 | | | | 0.2290 | 7.4 | 0.9894 | 0.2266 |
| 8.439 | 0.287 | | | | 0.2443 | 7.5 | 0.9880 | 0.2414 |
| 8.930 | 0.296 | | | | 0.2722 | 7.4 | 0.9866 | 0.2686 |
| 9.434 | 0.307 | | | | 0.2763 | 7.4 | 0.9852 | 0.2722 |
| 9.438 | 0.420 | | | | 0.2341 | 7.5 | 0.9852 | 0.2306 |
| 9.903 | 0.318 | | | | 0.2665 | 7.4 | 0.9762 | 0.2602 |

^a $^7\text{Li}(p;n)^7\text{Be}$ reaction.

^b ENDF/B-IV values (Ref. 25).

^c $\text{D}(d,n)^3\text{He}$ reaction.

TABLE 7. Eyeguide to the Available Experimental Cross Sections for the $^{204}\text{Pb}(n;n')^{204\text{m}}\text{Pb}$ Reaction

| E_n (MeV) | $\sigma_{nn'}$ (b) | E_n (MeV) | $\sigma_{nn'}$ (b) |
|----------------|-----------------------|----------------|-----------------------|
| 0.0 | 0.0 | 4.8 | 0.089 |
| 2.2 | 0.0 | 5.0 | 0.095 |
| 2.3 | 1.0×10^{-5} | 5.5 | 0.112 |
| 2.4 | 6.2×10^{-4} | 6.0 | 0.13 |
| 2.5 | 2.85×10^{-3} | 6.5 | 0.15 |
| 2.6 | 5.5×10^{-3} | 7.0 | 0.171 |
| 2.7 | 9.0×10^{-3} | 7.5 | 0.195 |
| 2.8 | 0.013 | 8.0 | 0.22 |
| 2.9 | 0.0173 | 8.5 | 0.242 |
| 3.0 | 0.022 | 9.0 | 0.26 |
| 3.1 | 0.026 | 9.5 | 0.263 |
| 3.2 | 0.03 | 10.0 | 0.255 |
| 3.3 | 0.034 | 11.0 | 0.19 |
| 3.4 | 0.038 | 12.0 | 0.12 |
| 3.5 | 0.042 | 12.9 | 0.081 |
| 3.6 | 0.046 | 14.2 | 0.063 |
| 3.7 | 0.05 | 15.1 | 0.057 |
| 3.8 | 0.053 | 16.6 | 0.042 |
| 3.9 | 0.057 | 17.8 | 0.033 |
| 4.0 | 0.061 | 20.0 | 0.02 |
| 4.2 | 0.068 | | |
| 4.4 | 0.075 | | |
| 4.6 | 0.082 | | |

TABLE 8. Sources of Systematic Error in the
 $^{204}\text{Pb}(n;n'\gamma)^{204}\text{Pb}$ Reaction Measurements

| Source of Error | Magnitude (%) |
|--|---------------|
| 1. Gamma-ray detector efficiency | 4 |
| 2. Geometric considerations | 3 |
| 3. Neutron-source properties | 2 |
| 4. Gamma-ray absorption and scattering | 0.5-3 |
| 5. Mass of uranium deposit | 1 |
| 6. Neutron absorption and scattering | <2 |

TABLE 9. Gamma-Ray Transitions Observed in the $^{204}\text{Pb}(n;n'\gamma)^{204}\text{Pb}$ Measurements for $E_n \lesssim 3$ MeV

| Transition | Measured Energy ^a (MeV) | Probable ^b Origin |
|------------|---------------------------------------|---------------------------------|
| 1 | 0.2894 ± 0.0003 | 1.5628 (0.2889) 1.2739 |
| 2 | 0.3307 ± 0.0004 | unknown |
| 3 | 0.3618 ± 0.0013 | 2.634 (0.366) 2.268 ? |
| 4 | 0.3750 ± 0.0007 | 1.2739 (0.3748) 0.89915 |
| 5 | 0.4518 ± 0.0004 | 1.353 (0.45385) 0.89915 |
| 6 | 0.6841 ± 0.0002 | 1.584 (0.6849) 0.89915 |
| 7 | 0.7059 ± 0.0004 | unknown |
| 8 | 0.7660 ± 0.0004 | 1.663 (0.76385) 0.89915 |
| 9 | 0.7822 ± 0.0005 | unknown |
| 10 | 0.8618 ± 0.0004 | 2.9285 (0.8636) 2.0649 ? |
| 11 | 0.8994 ± 0.0002 | 0.89915 (0.89915) 0 |
| 12 | 0.9187 ± 0.0004 | 1.8174 (0.9183) 0.89915 |
| 13 | 0.9839 ± 0.0003 | 2.2578 (0.9839) 1.2739 |
| 14 | 1.0493 ± 0.0006 | unknown |
| 15 | 1.0617 ± 0.0004 | 2.642 (1.058) 1.584 ? |
| 16 | 1.2588 ± 0.0006 | 2.9195 (1.2565) 1.663 ? |
| 17 | 1.2760 ± 0.0006 | 2.634 (1.281) 1.353 ? |
| 18 | 1.3514 ± 0.0003 | 1.353 (1.353) 0 |
| 19 | 1.5017 ± 0.0005 | unknown |
| 20 | 1.6663 ± 0.0004 | unknown |
| 21 | 1.6820 ± 0.0005 | unknown |
| 22 | 1.7223 ± 0.0004 | unknown |
| 23 | 1.7619 ± 0.0005 | unknown |
| 24 | 1.8732 ± 0.0005 | unknown |
| 25 | 1.9341 ± 0.0004 | 1.932 (1.932) 0 |

^aEnergies measured in the present experiment. Only the peak-location error is indicated.

^bOrigin Level (Transition) Terminal Level: Energies in MeV correspond to level scheme adopted in Ref. 9.

?Assignments are based on limited evidence and are uncertain.

TABLE 10. Experimental Cross Section Ratios and Calculated Cross Sections for Several Gamma-Ray Transitions Observed in the $^{204}\text{Pb}(n;n'\gamma)^{204}\text{Pb}$ Reaction^a

| Transition | E_γ (MeV) | E_n (MeV) | Resolution (MeV) | Ratio ($\sigma_{nn'\gamma}/\sigma_f$) | Ratio Error ^b (%) | σ_f^c (b) | $\sigma_{nn'\gamma}$ (b) | | |
|-------------|---------------------|-----------------------|---------------------|--|---------------------------------|---------------------|-----------------------------|----------------------|--------|
| 1 ↓ 2 | 0.2894 | 1.942 | 0.123 | 0.07951 | | | | | |
| | | 1.992 | 0.122 | 0.07133 | 25.7 | 1.269 | 0.1009 | | |
| | | 2.042 | 0.120 | 0.1096 | 20.9 | 1.270 | 0.09059 | | |
| | | 2.142 | 0.118 | 0.1205 | 25.7 | 1.271 | 0.1393 | | |
| | | 2.242 | 0.116 | 0.1812 | 25.7 | 1.274 | 0.1535 | | |
| | | 2.344 | 0.114 | 0.1350 | 25.7 | 1.276 | 0.2312 | | |
| | | 2.444 | 0.112 | 0.1084 | 30.6 | 1.278 | 0.1725 | | |
| | | 2.495 | 0.111 | 0.1220 | 30.6 | 1.281 | 0.1389 | | |
| | | 2.546 | 0.110 | 0.1348 | 16.2 | 1.282 | 0.1564 | | |
| | | 2.746 | 0.106 | 0.09952 | 30.6 | 1.277 | 0.1722 | | |
| | | 2.849 | 0.105 | 0.1570 | 30.6 | 1.259 | 0.1253 | | |
| | | 2.949 | 0.103 | 0.1048 | 20.9 | 1.250 | 0.1963 | | |
| | | 2.999 | 0.102 | 0.1260 | 25.7 | 1.240 | 0.1300 | | |
| | | 3 ↓ 4 ↓ 5 | 0.3307 | 1.837 | 0.125 | 0.09274 | 11.7 | 1.236 | 0.1557 |
| | | | | 1.989 | 0.122 | 0.03865 | 20.9 | 1.267 | 0.1175 |
| 2.444 | 0.112 | | | 0.09602 | 25.7 | 1.270 | 0.04909 | | |
| 2.495 | 0.111 | | | 0.07592 | 30.6 | 1.281 | 0.1230 | | |
| 2.546 | 0.110 | | | 0.08958 | 25.7 | 1.282 | 0.09733 | | |
| 2.999 | 0.102 | | | 0.04458 | 25.7 | 1.277 | 0.1144 | | |
| 0.3618 | 2.949 | | | 0.103 | 0.07445 | 30.6 | 1.236 | 0.05510 | |
| | 2.999 | | | 0.102 | 0.04704 | 30.6 | 1.240 | 0.09232 | |
| | 1.990 | | | 0.122 | 0.07628 ^d | 30.6 | 1.236 | 0.09232 | |
| | 2.040 | | | 0.120 | 0.08285 ^d | 20.9 | 1.236 | 0.05814 ^d | |
| | 2.242 | | | 0.116 | 0.1143 ^d | 20.9 | 1.270 | 0.09687 ^d | |
| | 2.495 | | | 0.111 | 0.06418 ^d | 20.9 | 1.271 | 0.1053 ^d | |
| | 2.646 | | | 0.108 | 0.06091 ^d | 25.7 | 1.276 | 0.1458 ^d | |
| | 2.949 | | | 0.103 | 0.09508 ^d | 25.7 | 1.282 | 0.08228 ^d | |
| | 2.999 | | | 0.102 | 0.06594 ^d | 30.6 | 1.268 | 0.07723 ^d | |
| | 0.3750 | 1.838 | 0.125 | 0.09976 | 25.7 | 1.282 | 0.08228 ^d | | |
| | | 1.990 | 0.122 | 0.07198 | 25.7 | 1.268 | 0.07723 ^d | | |
| | | 1.990 | 0.122 | 0.07198 | 25.7 | 1.240 | 0.1179 ^d | | |
| | | 1.838 | 0.125 | 0.06594 ^d | 20.9 | 1.240 | 0.1179 ^d | | |
| | | 1.990 | 0.122 | 0.09976 | 25.7 | 1.236 | 0.08150 ^d | | |
| | | 1.838 | 0.125 | 0.06594 ^d | 20.9 | 1.267 | 0.1264 | | |
| 1.990 | | 0.122 | 0.07198 | 25.7 | 1.270 | 0.09141 | | | |

TABLE 10 (Contd.)

| Transition | E_{γ} (MeV) | E_n (MeV) | Resolution (MeV) | Ratio ($\sigma_{nn'\gamma}/\sigma_f$) | Ratio Error ^b (%) | σ_f^c (b) | $\sigma_{nn'\gamma}$ (b) |
|-------------|-----------------------|----------------|---------------------|--|---------------------------------|---------------------|-----------------------------|
| 5 ↓ 6 | 0.4518 | 2.343 | 0.114 | 0.06347 | 30.6 | 1.278 | 0.08112 |
| | | 2.495 | 0.111 | 0.07204 | 20.9 | 1.282 | 0.09235 |
| | | 2.849 | 0.105 | 0.08520 | 25.7 | 1.250 | 0.1065 |
| | | 2.949 | 0.103 | 0.1000 | 25.7 | 1.240 | 0.1240 |
| | | 2.999 | 0.102 | 0.06133 | 16.2 | 1.236 | 0.07581 |
| | | 1.745 | 0.128 | 0.1639 | 25.7 | 1.265 | 0.2073 |
| | | 1.839 | 0.125 | 0.1222 | 20.9 | 1.267 | 0.1548 |
| | | 1.940 | 0.123 | 0.1224 | 20.9 | 1.269 | 0.1553 |
| | | 1.990 | 0.122 | 0.1139 | 16.2 | 1.270 | 0.1446 |
| | | 2.041 | 0.120 | 0.1611 | 20.9 | 1.271 | 0.2048 |
| 6 ↓ 7 | 0.6841 | 2.141 | 0.118 | 0.1422 | 25.7 | 1.274 | 0.1811 |
| | | 2.242 | 0.116 | 0.1648 | 25.7 | 1.276 | 0.2103 |
| | | 2.343 | 0.114 | 0.1354 | 25.7 | 1.278 | 0.1731 |
| | | 2.444 | 0.112 | 0.2143 | 20.9 | 1.281 | 0.2745 |
| | | 2.495 | 0.111 | 0.1594 | 11.7 | 1.282 | 0.2044 |
| | | 2.546 | 0.110 | 0.1637 | 20.9 | 1.277 | 0.2091 |
| | | 2.647 | 0.108 | 0.1482 | 25.7 | 1.268 | 0.1879 |
| | | 2.747 | 0.106 | 0.1855 | 20.9 | 1.259 | 0.2335 |
| | | 2.849 | 0.105 | 0.2141 | 20.9 | 1.250 | 0.2676 |
| | | 2.949 | 0.103 | 0.1980 | 20.9 | 1.240 | 0.2455 |
| 7 ↓ 8 | 0.7059 | 2.999 | 0.102 | 0.1629 | 7.8 | 1.236 | 0.2013 |
| | | 1.736 | 0.128 | 0.06048 | 30.6 | 1.265 | 0.07651 |
| | | 2.242 | 0.116 | 0.08174 | 30.6 | 1.276 | 0.1043 |
| | | 2.647 | 0.108 | 0.1098 | 30.6 | 1.268 | 0.1392 |
| | | 2.949 | 0.103 | 0.08113 | 30.6 | 1.240 | 0.1006 |
| 8 ↓ | 0.7660 | 2.999 | 0.102 | 0.08908 | 11.7 | 1.236 | 0.1101 |
| | | 1.945 | 0.123 | 0.08006 | 25.7 | 1.269 | 0.1016 |
| | | 1.993 | 0.122 | 0.04349 | 20.9 | 1.270 | 0.05523 |
| | | 2.496 | 0.111 | 0.06466 | 16.2 | 1.282 | 0.08290 |
| | | 2.849 | 0.105 | 0.1182 | 25.7 | 1.250 | 0.1478 |
| | | 2.949 | 0.103 | 0.09718 | 30.6 | 1.240 | 0.1205 |
| | | 2.999 | 0.102 | 0.07528 | 11.7 | 1.236 | 0.09304 |

TABLE 10 (Contd.)

| Transition | E_{γ} (MeV) | E_n (MeV) | Resolution (MeV) | Ratio ($\sigma_{nn'\gamma}/\sigma_f$) | Ratio Error ^b (%) | σ_f^c (b) | $\sigma_{nn'\gamma}$ (b) |
|--------------|-----------------------|----------------|---------------------|--|---------------------------------|---------------------|-----------------------------|
| 9 ↓ 11 | 0.7822 ↓ 0.8994 | 1.989 | 0.122 | 0.05835 | 20.9 | 1.270 | 0.07410 |
| | | 2.495 | 0.111 | 0.04768 | 20.9 | 1.282 | 0.06112 |
| | | 2.949 | 0.103 | 0.07348 | 30.6 | 1.240 | 0.09112 |
| | | 2.999 | 0.102 | 0.06201 | 16.2 | 1.236 | 0.07664 |
| | | 0.967 | 0.159 | 0.2687 | 16.2 | 1.195 | 0.3211 |
| | | 1.001 | 0.156 | 0.1916 | 11.7 | 1.209 | 0.2317 |
| | | 1.037 | 0.154 | 0.2667 | 13.4 | 1.224 | 0.3264 |
| | | 1.130 | 0.149 | 0.3556 | 11.7 | 1.251 | 0.4448 |
| | | 1.230 | 0.145 | 0.3998 | 11.7 | 1.253 | 0.5009 |
| | | 1.331 | 0.141 | 0.4279 | 11.7 | 1.255 | 0.5370 |
| | | 1.432 | 0.138 | 0.4355 | 11.7 | 1.258 | 0.5479 |
| | | 1.483 | 0.136 | 0.4569 | 7.8 | 1.259 | 0.5752 |
| | | 1.534 | 0.134 | 0.4687 | 11.7 | 1.260 | 0.5906 |
| | | 1.635 | 0.131 | 0.5345 | 11.7 | 1.262 | 0.6746 |
| | | 1.736 | 0.128 | 0.5240 | 10 | 1.265 | 0.6628 |
| | | 1.837 | 0.125 | 0.6163 | 10 | 1.267 | 0.7809 |
| | | 1.939 | 0.123 | 0.6657 | 10 | 1.269 | 0.8448 |
| | | 1.990 | 0.122 | 0.6554 | 7.8 | 1.270 | 0.8324 |
| | | 2.041 | 0.120 | 0.6859 | 10 | 1.271 | 0.8718 |
| | | 2.041 | 0.120 | 0.6859 | 10 | 1.271 | 0.8718 |
| | | 2.141 | 0.118 | 0.6294 | 11.7 | 1.274 | 0.8018 |
| | | 2.242 | 0.116 | 0.7276 | 11.7 | 1.276 | 0.9284 |
| | | 2.343 | 0.114 | 0.8114 | 11.7 | 1.278 | 1.037 |
| | | 2.444 | 0.112 | 0.8126 | 10 | 1.281 | 1.041 |
| | | 2.496 | 0.111 | 0.7749 | 7.8 | 1.282 | 0.9934 |
| | | 2.546 | 0.110 | 0.8528 | 10 | 1.277 | 1.089 |
| | | 2.647 | 0.108 | 0.9132 | 10 | 1.268 | 1.158 |
| | | 2.747 | 0.106 | 0.9102 | 10 | 1.259 | 1.146 |
| 2.849 | 0.105 | 0.9632 | 7.8 | 1.250 | 1.204 | | |
| 2.949 | 0.103 | 1.014 | 7.8 | 1.240 | 1.257 | | |
| 2.999 | 0.102 | 0.9191 | 7.8 | 1.236 | 1.136 | | |

TABLE 10 (Contd.)

| Transition | E_{γ} (MeV) | E_n (MeV) | Resolution (MeV) | Ratio ($\sigma_{nn'\gamma}/\sigma_f$) | Ratio Error ^b (%) | σ_f^c (b) | $\sigma_{nn'\gamma}$ (b) |
|------------|-----------------------|----------------|---------------------|--|---------------------------------|---------------------|-----------------------------|
| 12 | 0.9187 | 2.243 | 0.116 | 0.1010 | 25.7 | 1.276 | 0.1289 |
| | | 2.495 | 0.111 | 0.06947 | 16.2 | 1.282 | 0.08906 |
| | | 2.647 | 0.108 | 0.1006 | 25.7 | 1.268 | 0.1275 |
| | | 2.747 | 0.106 | 0.07841 | 25.7 | 1.259 | 0.09872 |
| | | 2.849 | 0.105 | 0.1081 | 25.7 | 1.250 | 0.1351 |
| 13 | 0.9839 | 2.949 | 0.103 | 0.1122 | 25.7 | 1.240 | 0.1391 |
| | | 2.999 | 0.102 | 0.05930 | 16.2 | 1.236 | 0.07329 |
| | | 2.649 | 0.108 | 0.1021 | 25.7 | 1.268 | 0.1294 |
| | | 2.748 | 0.106 | 0.09110 | 20.9 | 1.259 | 0.1147 |
| | | 2.850 | 0.105 | 0.1374 | 20.9 | 1.250 | 0.1717 |
| 15 | 1.0617 | 2.950 | 0.103 | 0.1406 | 20.9 | 1.240 | 0.1743 |
| | | 3.000 | 0.102 | 0.1450 | 11.7 | 1.236 | 0.1792 |
| 18 | 1.3514 | 2.999 | 0.102 | 0.06675 | 16.2 | 1.236 | 0.08250 |
| | | 1.499 | 0.136 | 0.09587 | 16.2 | 1.259 | 0.1207 |
| | | 1.543 | 0.134 | 0.1695 | 20.9 | 1.260 | 0.2136 |
| | | 1.638 | 0.131 | 0.1426 | 20.9 | 1.262 | 0.1800 |
| | | 1.738 | 0.128 | 0.1366 | 20.9 | 1.265 | 0.1728 |
| | | 1.838 | 0.125 | 0.1938 | 16.2 | 1.267 | 0.2455 |
| | | 1.940 | 0.123 | 0.1707 | 20.9 | 1.269 | 0.2166 |
| | | 1.990 | 0.122 | 0.1831 | 11.7 | 1.270 | 0.2325 |
| | | 2.040 | 0.120 | 0.1752 | 20.9 | 1.271 | 0.2227 |
| | | 2.141 | 0.118 | 0.1736 | 20.9 | 1.274 | 0.2212 |
| | | 2.242 | 0.116 | 0.1856 | 20.9 | 1.276 | 0.2368 |
| | | 2.343 | 0.114 | 0.1949 | 20.9 | 1.278 | 0.2491 |
| | | 2.445 | 0.112 | 0.2077 | 20.9 | 1.281 | 0.2660 |
| | | 2.496 | 0.111 | 0.2018 | 11.7 | 1.282 | 0.2587 |
| | | 2.546 | 0.110 | 0.2159 | 20.9 | 1.277 | 0.2757 |
| | | 2.647 | 0.108 | 0.2302 | 20.9 | 1.268 | 0.2919 |
| | | 2.747 | 0.106 | 0.2563 | 16.2 | 1.259 | 0.3227 |
| | | 2.849 | 0.105 | 0.2665 | 16.2 | 1.250 | 0.3331 |
| | | 2.949 | 0.103 | 0.2428 | 16.2 | 1.240 | 0.3011 |
| | | 2.999 | 0.102 | 0.2653 | 7.8 | 1.236 | 0.3279 |

TABLE 10 (Contd.)

| Transition | E_{γ} (MeV) | E_n (MeV) | Resolution (MeV) | Ratio ($\sigma_{nn'\gamma}/\sigma_f$) | Ratio Error ^b (%) | σ_f^c (b) | $\sigma_{nn'\gamma}$ (b) |
|------------|-----------------------|----------------|---------------------|--|---------------------------------|---------------------|-----------------------------|
| 20 | 1.6663 | 2.999 | | | | | |
| 21 | 1.6820 | 2.495 | 0.102 | 0.06074 | 20.9 | 1.236 | 0.07507 |
| ↓ | ↓ | 2.999 | 0.111 | 0.06700 | 20.9 | 1.282 | 0.08589 |
| 22 | 1.7223 | 2.999 | 0.102 | 0.05046 | 20.9 | 1.236 | 0.06237 |
| 23 | 1.7619 | 2.495 | 0.111 | 0.04452 | 20.9 | 1.236 | 0.06749 |
| ↓ | ↓ | 2.999 | 0.102 | 0.04070 | 25.7 | 1.282 | 0.05708 |
| 24 | 1.8732 | 2.949 | 0.103 | 0.08266 | 25.7 | 1.236 | 0.05030 |
| ↓ | ↓ | 2.999 | 0.102 | 0.06394 | 30.6 | 1.240 | 0.1025 |
| 25 | 1.9341 | 2.999 | 0.102 | 0.03402 | 20.9 | 1.236 | 0.07903 |
| | | | | | 30.6 | 1.236 | 0.04205 |

^aRatio and cross section values are angle-integrated. Integrated values were derived from measured differential values using Eq. 1 (Sec. III.C). Fission cross sections are for ^{235}U .

^bError includes gamma-ray yield uncertainty combined with an overall systematic error of ~6% (see Table 8).

^cDerived from ENDF/B-IV (Ref. 25).

^dThe 1.2739-MeV level is an isomer with $t_{1/2} = 0.29 \mu\text{sec}$. Therefore, measured cross section is less than true production cross section (Sec. III.2 C).

TABLE 11. Measured Angular Distributions for the 0.8994-MeV
Gamma Ray from the $^{204}\text{Pb}(n;n'\gamma)^{204}\text{Pb}$ Reaction

| θ (deg) | $\cos \theta$ (no dim.) | $[w(\theta)/w(90^\circ)]^a$ |
|-------------------|-------------------------|-----------------------------|
| $E_n = 1.037$ MeV | | |
| 30 | 0.8660 | 1.830 ± 0.275 |
| 40 | 0.7660 | 2.113 ± 0.317 |
| 50 | 0.6428 | 1.392 ± 0.279 |
| 60 | 0.5000 | 1.455 ± 0.291 |
| 70 | 0.3420 | 0.715 ± 0.178 |
| 80 | 0.1736 | 0.923 ± 0.185 |
| 90 | 0 | 1.094 ± 0.219 |
| 90 | 0 | 1.010 ± 0.202 |
| 100 | -0.1736 | 1.134 ± 0.170 |
| 110 | -0.3420 | 1.666 ± 0.250 |
| 120 | -0.5000 | 1.467 ± 0.220 |
| 130 | -0.6428 | 1.436 ± 0.215 |
| 135 | -0.7071 | 1.601 ± 0.240 |
| $E_n = 1.230$ MeV | | |
| 30 | 0.8660 | 1.911 ± 0.287 |
| 40 | 0.7660 | 1.564 ± 0.156 |
| 50 | 0.6428 | 1.403 ± 0.210 |
| 60 | 0.5000 | 1.193 ± 0.239 |
| 70 | 0.3420 | 0.890 ± 0.178 |
| 80 | 0.1736 | 1.060 ± 0.159 |
| 90 | 0 | 1.138 ± 0.228 |
| 90 | 0 | 0.987 ± 0.197 |
| 100 | -0.1736 | 1.086 ± 0.163 |
| 110 | -0.3420 | 1.300 ± 0.195 |
| 120 | -0.5000 | 1.137 ± 0.170 |
| 130 | -0.6428 | 1.510 ± 0.151 |
| 135 | -0.7071 | 1.701 ± 0.170 |
| $E_n = 1.432$ MeV | | |
| 40 | 0.7660 | 1.313 ± 0.131 |
| 50 | 0.6428 | 1.159 ± 0.116 |
| 60 | 0.5000 | 1.207 ± 0.121 |
| 70 | 0.3420 | 1.089 ± 0.109 |
| 80 | 0.1736 | 0.845 ± 0.127 |
| 90 | 0 | 0.849 ± 0.127 |
| 90 | 0 | 1.053 ± 0.105 |
| 100 | -0.1736 | 1.058 ± 0.106 |
| 110 | -0.3420 | 1.174 ± 0.117 |
| 120 | -0.5000 | 1.153 ± 0.115 |
| 130 | -0.6428 | 1.063 ± 0.106 |
| 135 | -0.7071 | 1.262 ± 0.126 |

^aError includes only the uncertainty in the peak yield. Best fits of second-order Legendre polynomial expansions to the experimental distributions equal unity at 90° even though the experimental values given in this table fluctuate about unity near 90° .

TABLE 12. w_2 -Coefficients Corresponding to Fits of a Second-Order Legendre Polynomial Expansion to Measured Angular Distributions for the 0.8994-MeV Gamma-Ray Transition from the $^{204}\text{Pb}(n;n'\gamma)^{204}\text{Pb}$ Reaction^a

| E_n (MeV) | w_2^b (no dim.) |
|----------------|----------------------|
| 1.037 | 0.59 ± 0.45 |
| 1.230 | 0.54 ± 0.26 |
| 1.432 | 0.27 ± 0.10 |

^aExperimental data were fitted using Eq. (2).

^bError is the standard deviation in the best-fit value of w_2 derived from a least-squares analysis.

FIGURE CAPTIONS

- Fig. 1. Sample Irradiation Apparatus Used for the Present Set of Measurements. The gas target assembly shown was employed for irradiations with neutrons from the $D(d,n)^3\text{He}$ reaction. The lithium target assembly used for lower-energy irradiations is not shown. (ANL Neg. No. 116-2355 Rev. 1)
- Fig. 2. Gamma-ray Spectrum from ^{204m}Pb Decay Measured with a Ge(Li) Detector. (ANL Neg. No. 116-77-824).
- Fig. 3. Decay Scheme for ^{204m}Pb Derived from Ref. 9. (ANL Neg. No. 116-77-826).
- Fig. 4. Schematic Representation of Neutron Scattering Corrections. (ANL Neg. No. 116-1174).
- Fig. 5. Cross Sections for the $^{204}\text{Pb}(n;n')^{204m}\text{Pb}$ Reaction: Present Work (O) error bars do not include monitor cross section errors, Ref. 28 (X), Ref. 29 (\square), Ref. 30 (\diamond) and Ref. 31 (\times). Solid curve is an eye-guide sketched through the available data. (ANL Neg. No. 116-77-821).
- Fig. 6. Plots of Response of the $^{204}\text{Pb}(n;n')^{204m}\text{Pb}$ Reaction in a Uranium-235 Fission Neutron Spectrum. The cross section σ (SIG) and spectrum ϕ (not labelled) are shown in the first frame. The second frame gives the product $\sigma\phi$ (SIG*PHI) and it is easy to see that the region of largest response is $\sim 3-7$ MeV. The last frame is a plot of $\sigma'\phi$ (SIGP*PHI) where σ' is the energy derivative of the cross section. This curve indicates that the region of greatest sensitivity to the energy scale of σ is 2.5-5 MeV. (ANL Neg. No. 116-77-818).
- Fig. 7. Schematic Diagram of the Apparatus Used in the $^{204}\text{Pb}(n;n'\gamma)^{204}\text{Pb}$ Measurements. The sample geometry differs somewhat from that indicated in the figure (see Sec. III.A of the text). (ANL Neg. No. 116-2273)
- Fig. 8. Spectrum of Prompt Gamma Rays Resulting from the Irradiation of the ^{204}Pb -enriched Sample with ~ 3 -MeV Neutrons. (ANL Neg. No. 116-77-823).

Fig. 9. Level Scheme for ^{204}Pb Adapted from Ref. 9. Probable origin of several gamma-ray transitions observed in the present experiment is indicated. Identification of the transitions is based on Table 9. Transitions indicated by dashed lines are speculative. (ANL Neg. No. 116-77-825 Rev. 1).

Figs. 10-11. Cross-section Excitation Functions for Transitions Observed in the $^{204}\text{Pb}(n;n'\gamma)^{204}\text{Pb}$ Measurements. Data are listed in Table 10. (ANL Neg. Nos. 116-77-822 and 116-77-819 respectively).

Fig. 12. Measured Angular Distributions for the 0.8994-MeV Gamma-ray (Transition No. 11 in Table 9). Solid curves are best fits of second-order Legendre polynomial expansions to the experimental data. (ANL Neg. No. 116-77-820).

Fig. 13. Geometry Applicable to Neutron Scattering Calculations with Computer Program CYSCAT. (No negative available).

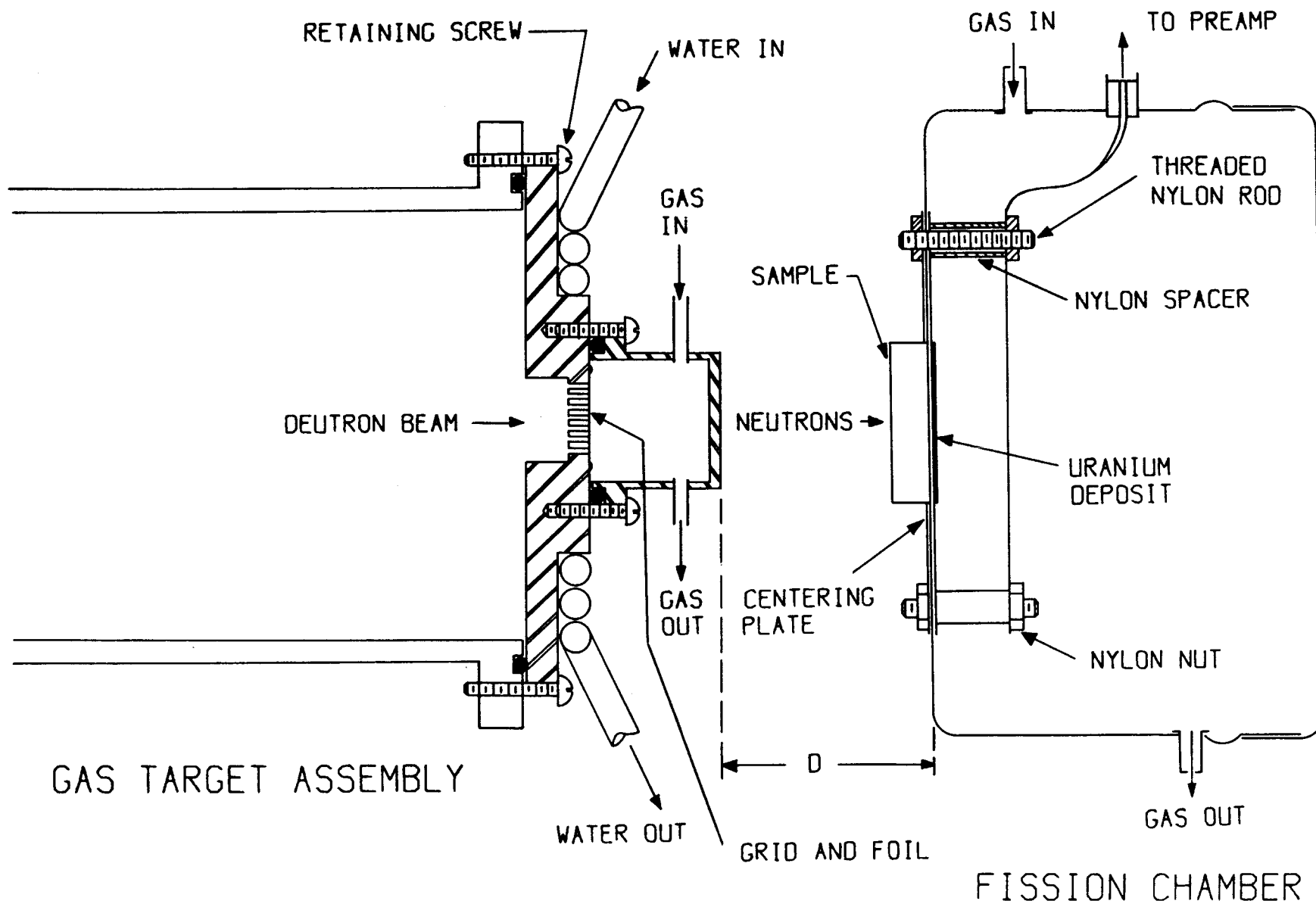


Fig. 1

Relative Yield

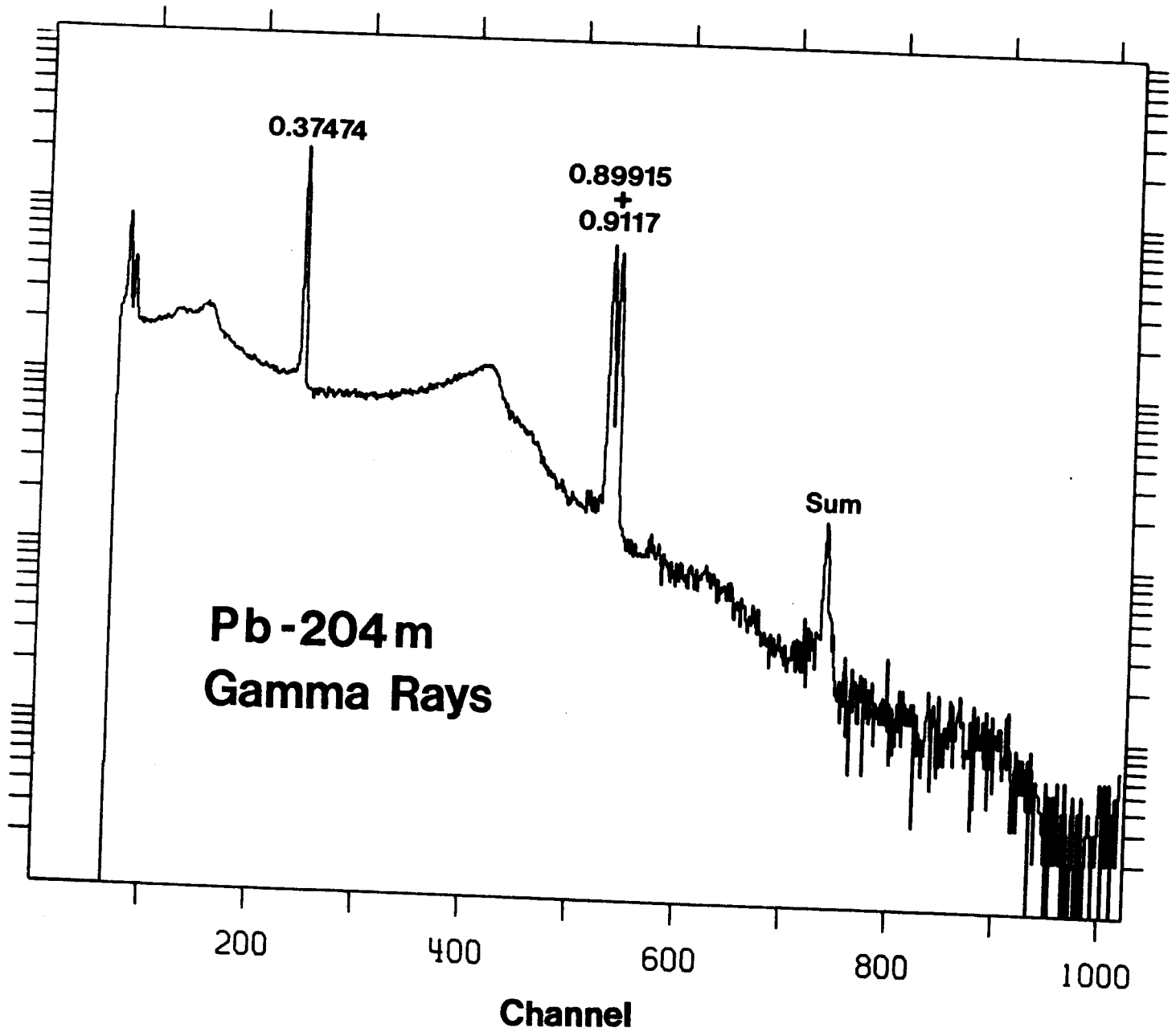


Fig. 2

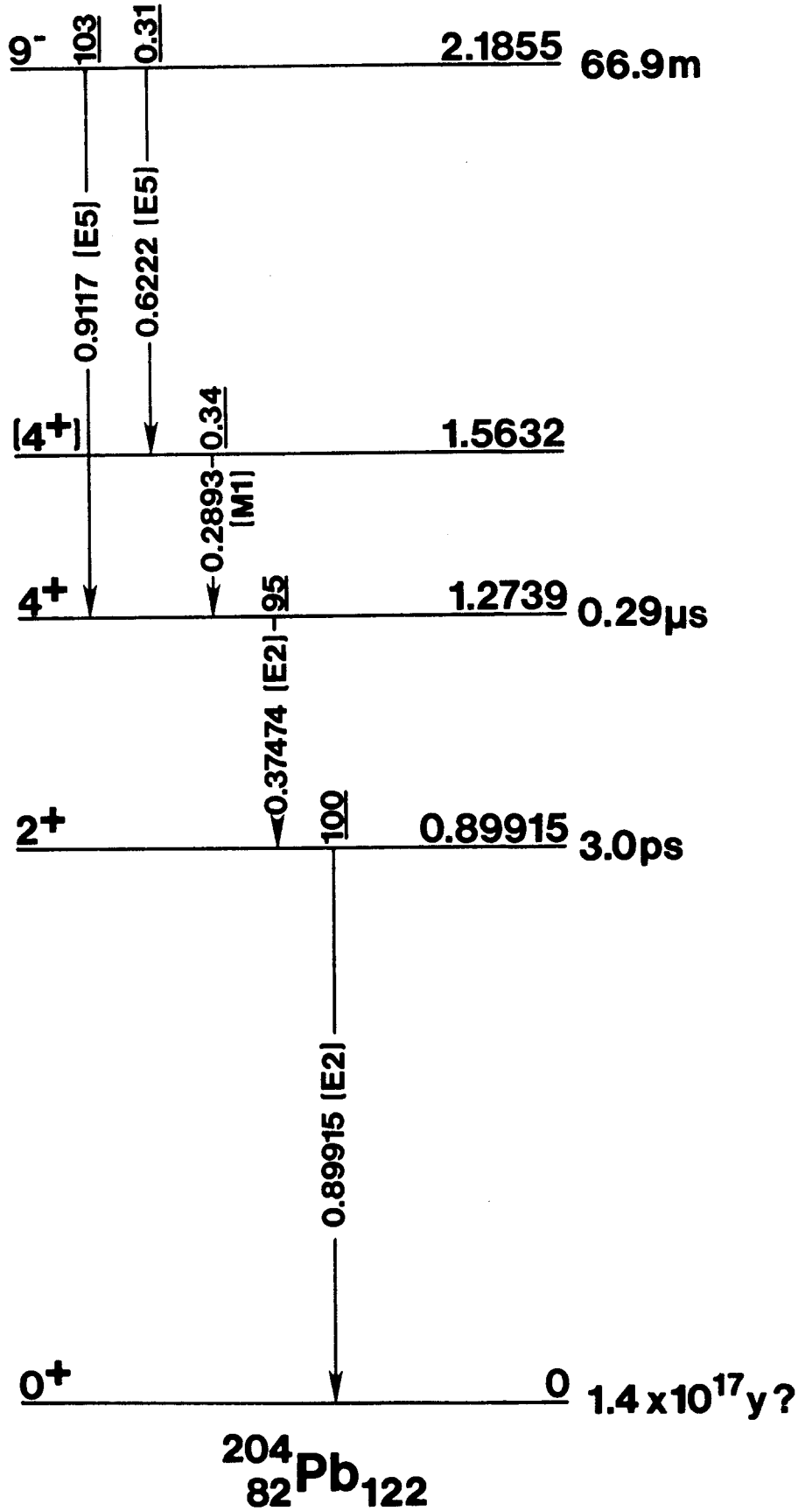


Fig. 3

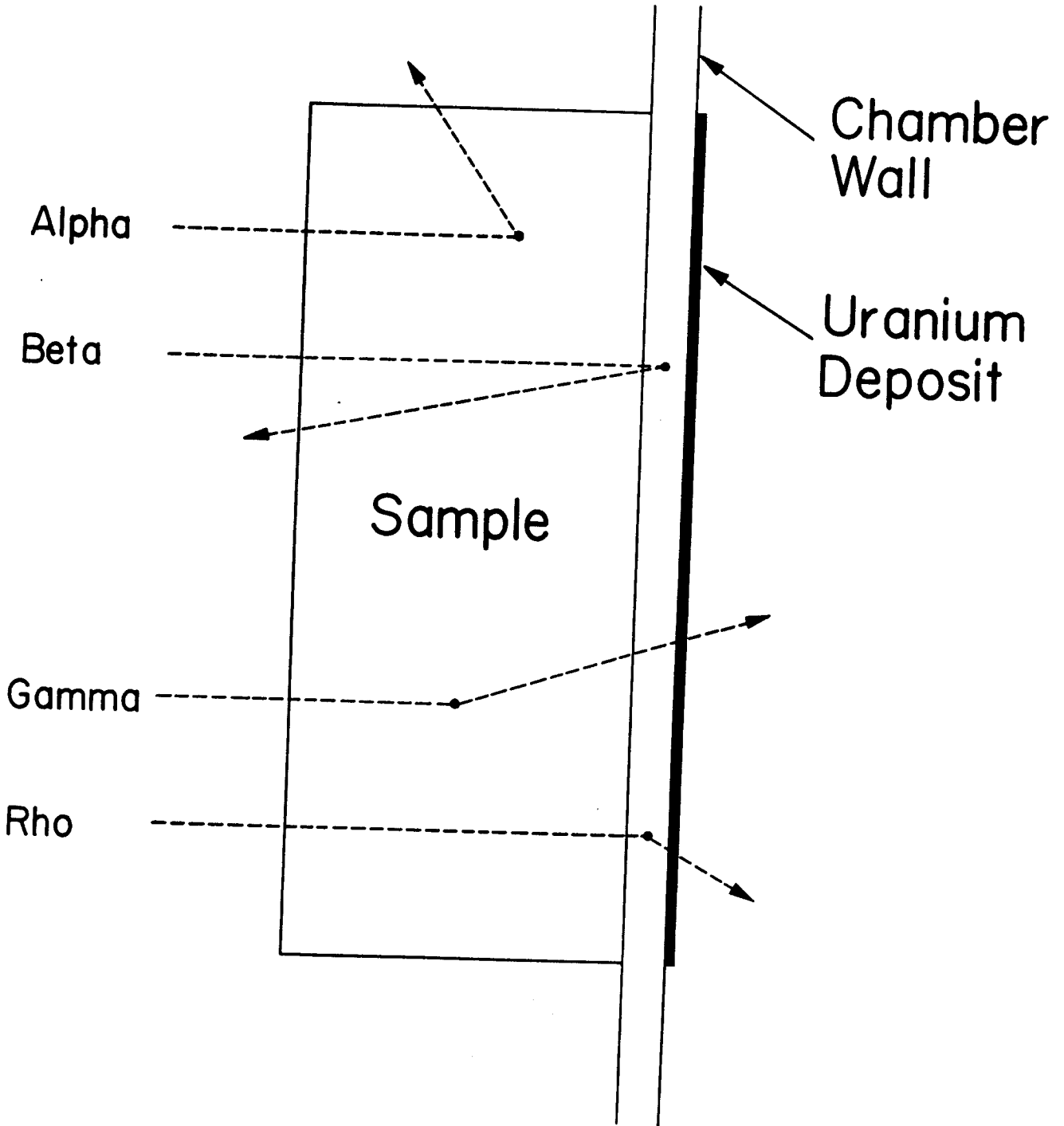


Fig. 4

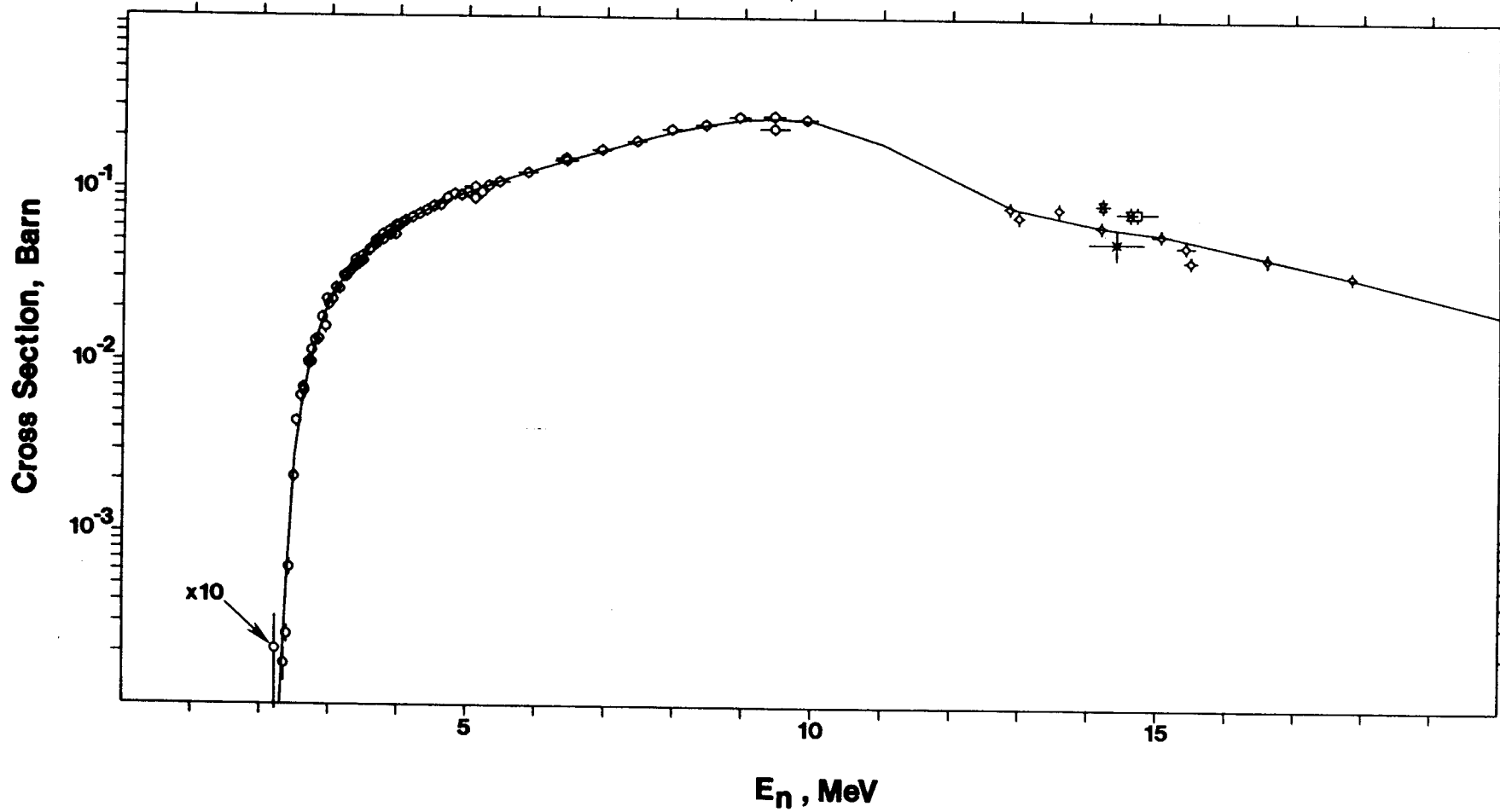


Fig. 5

PB-204 (N, N-) PB-204M
U-235 FISSION ENDF/B-IV

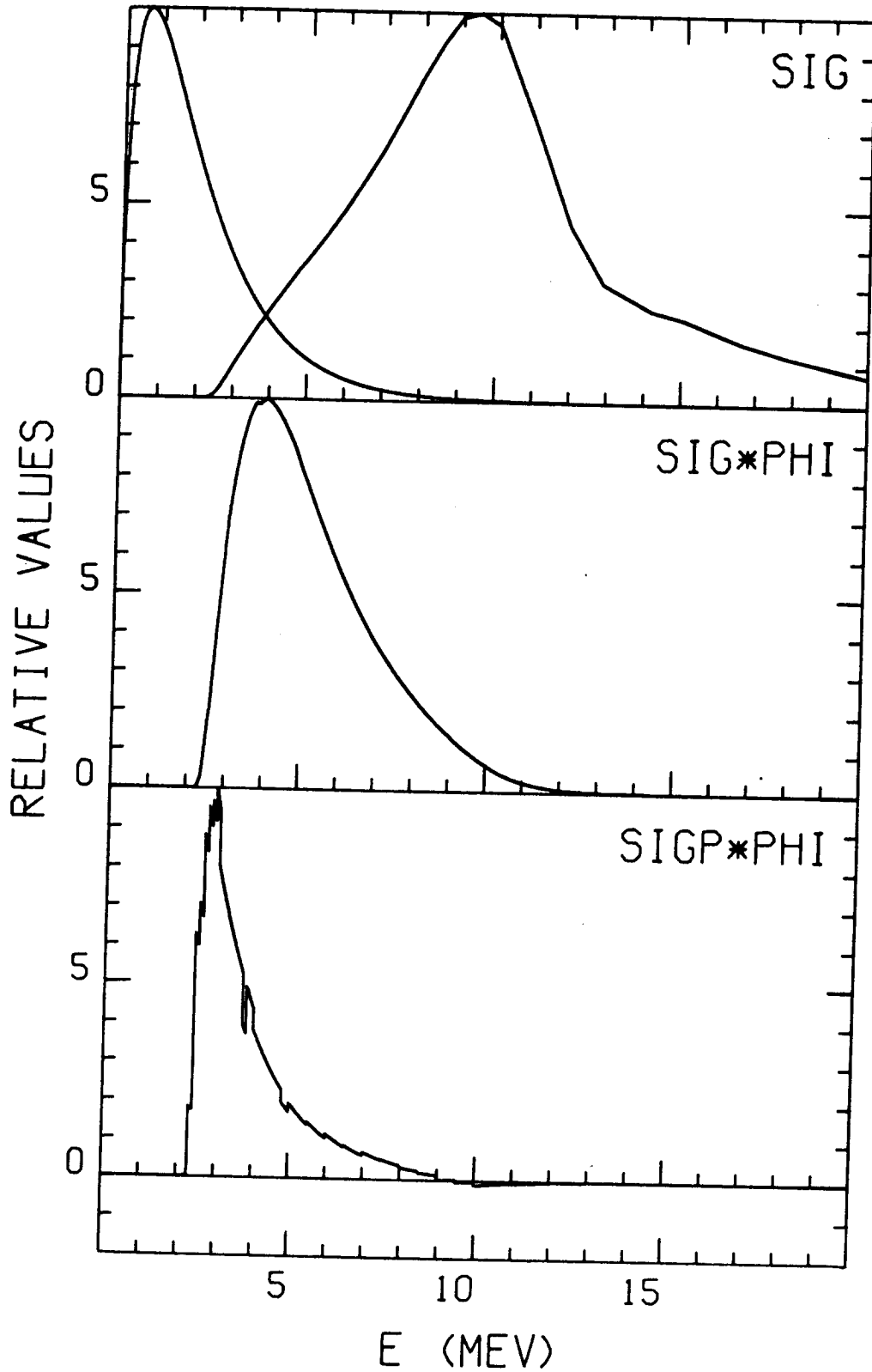


Fig. 6

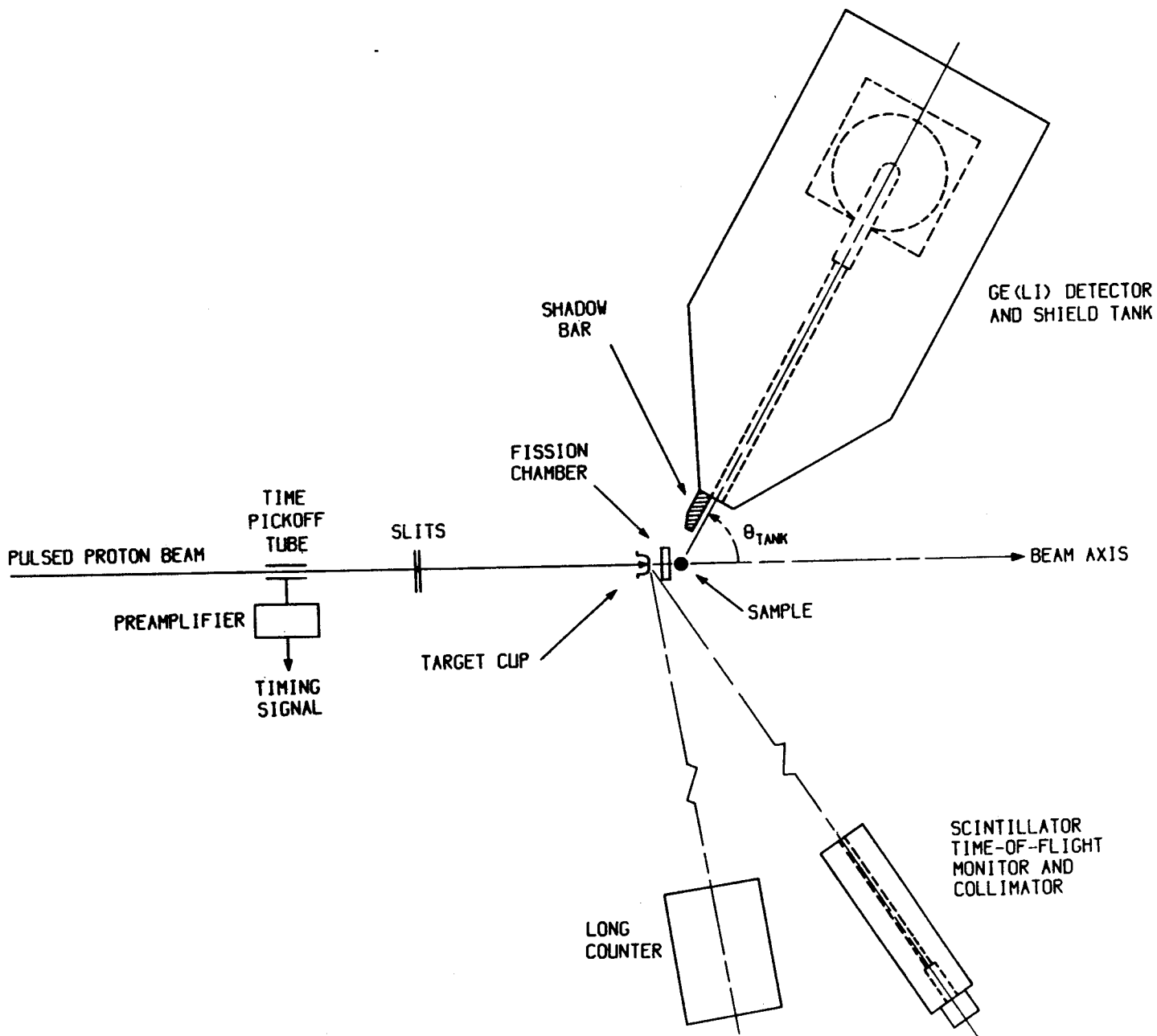


Fig. 7

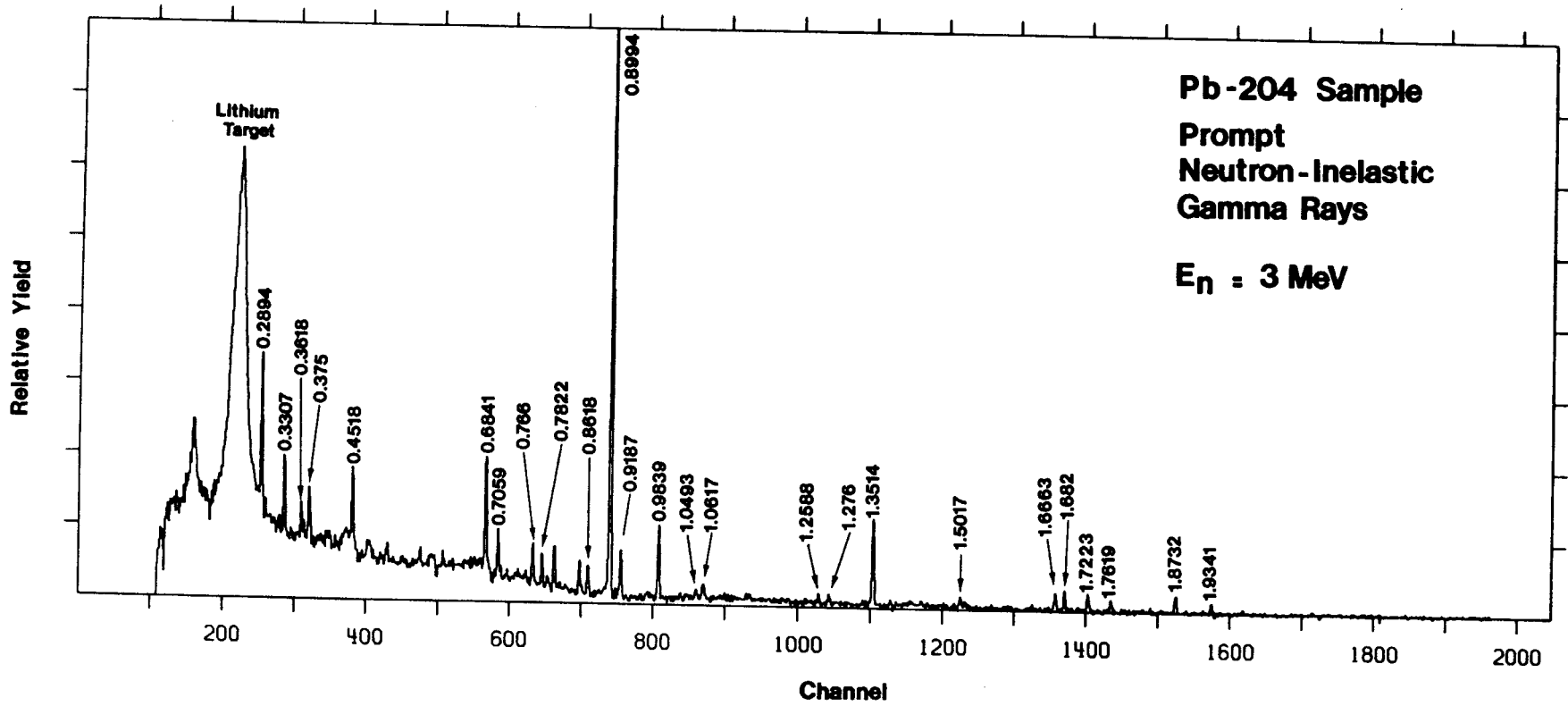
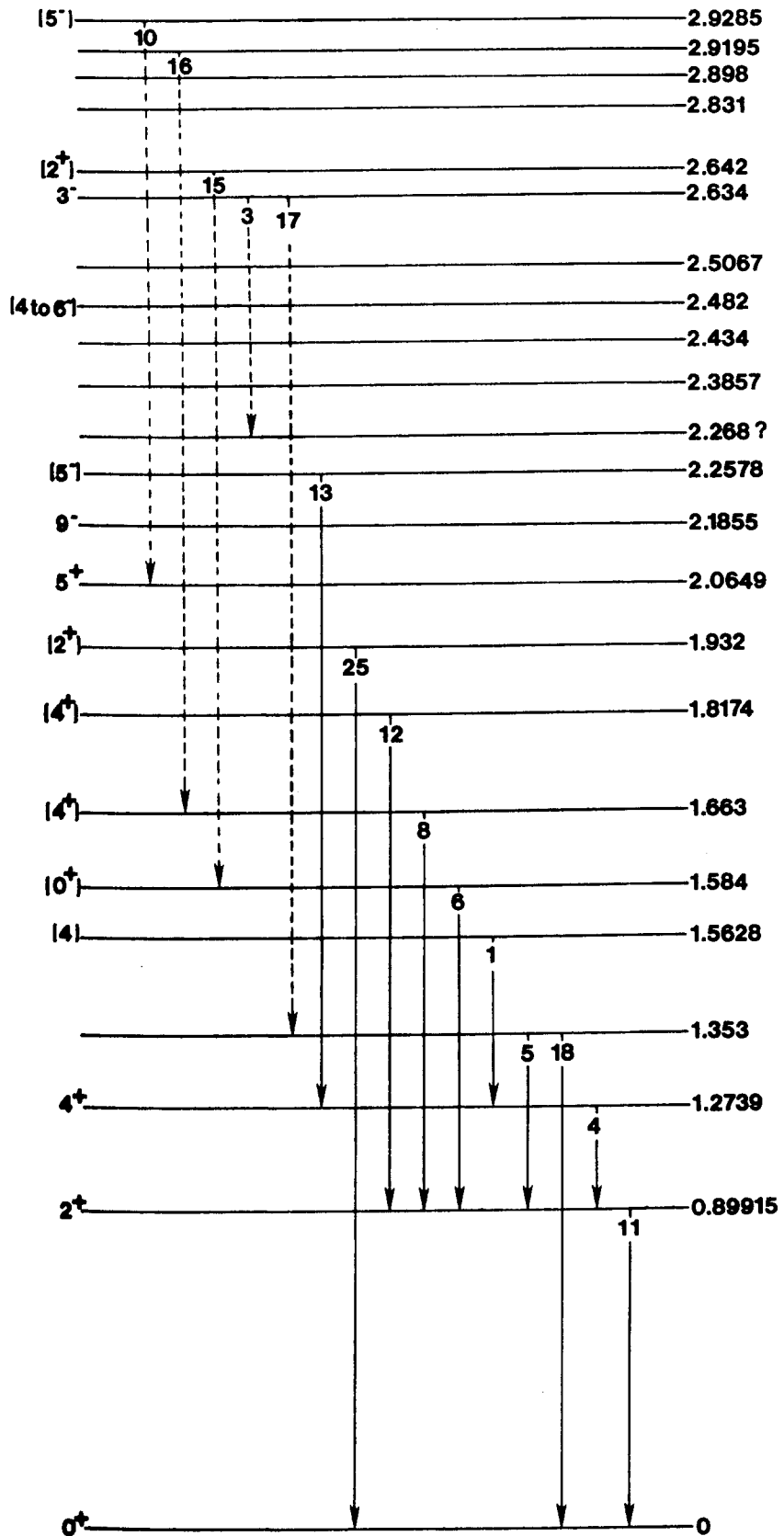


Fig. 8



$^{204}_{82}\text{Pb}_{122}$

Fig. 9

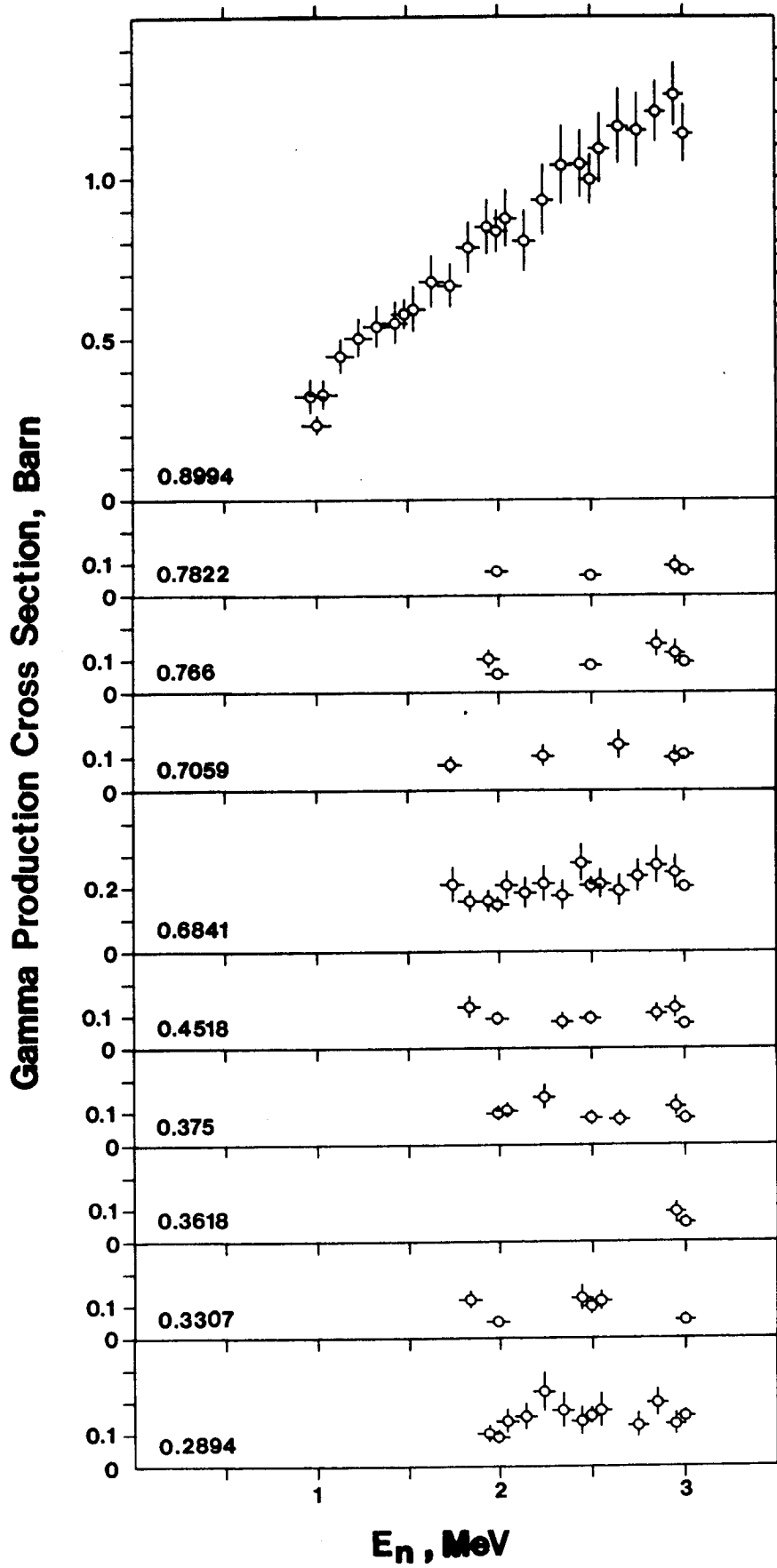


Fig. 10

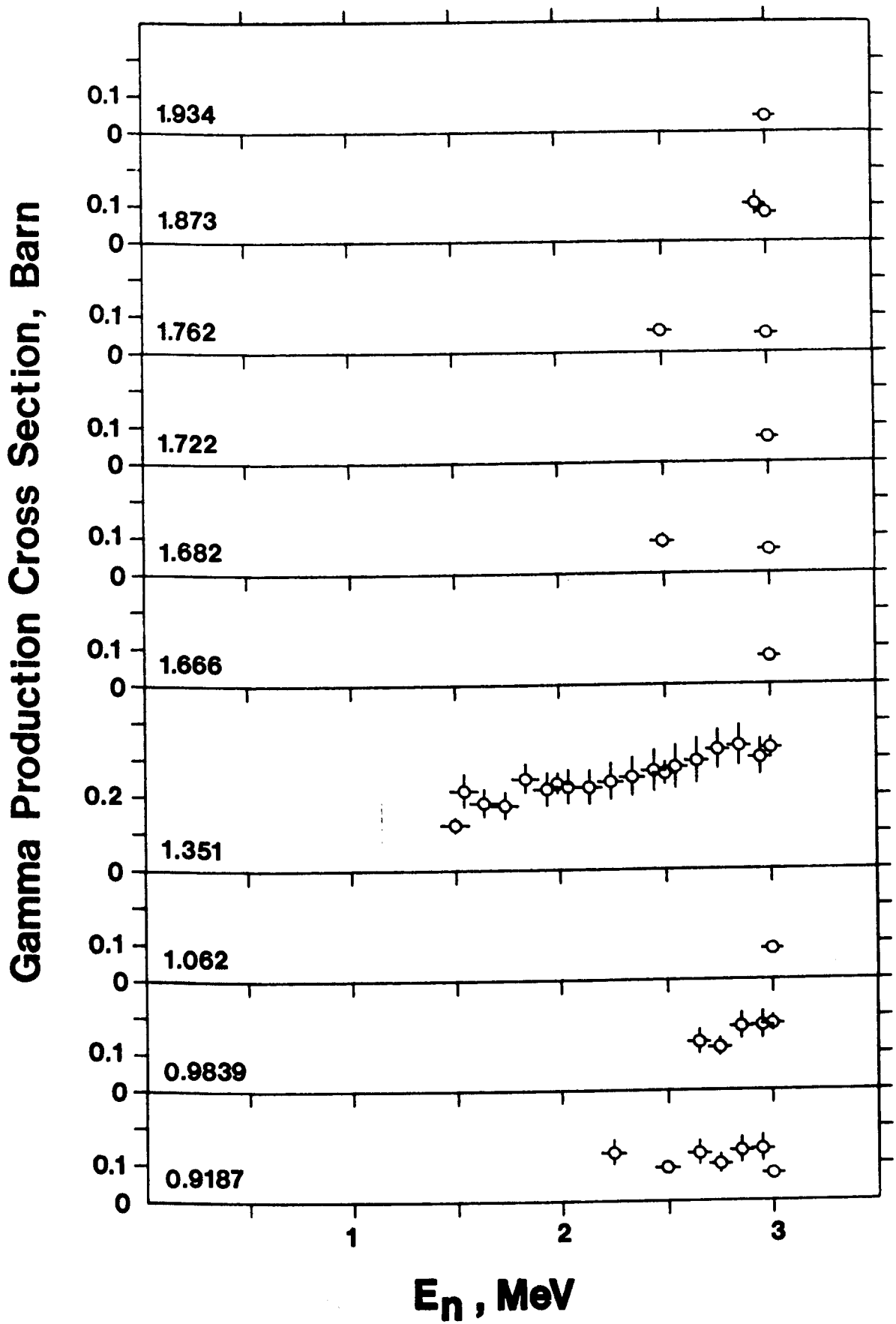


Fig. 11

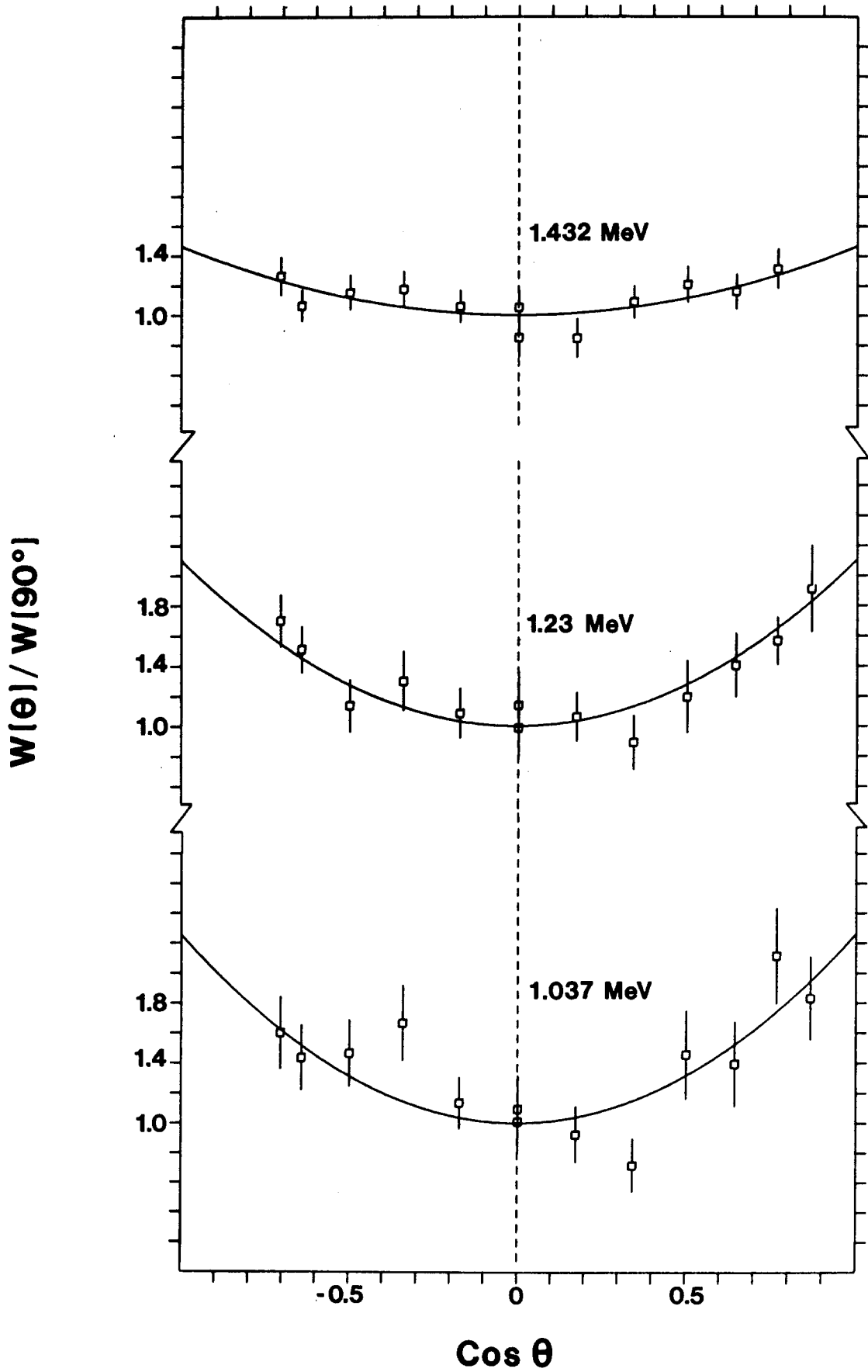


Fig. 12

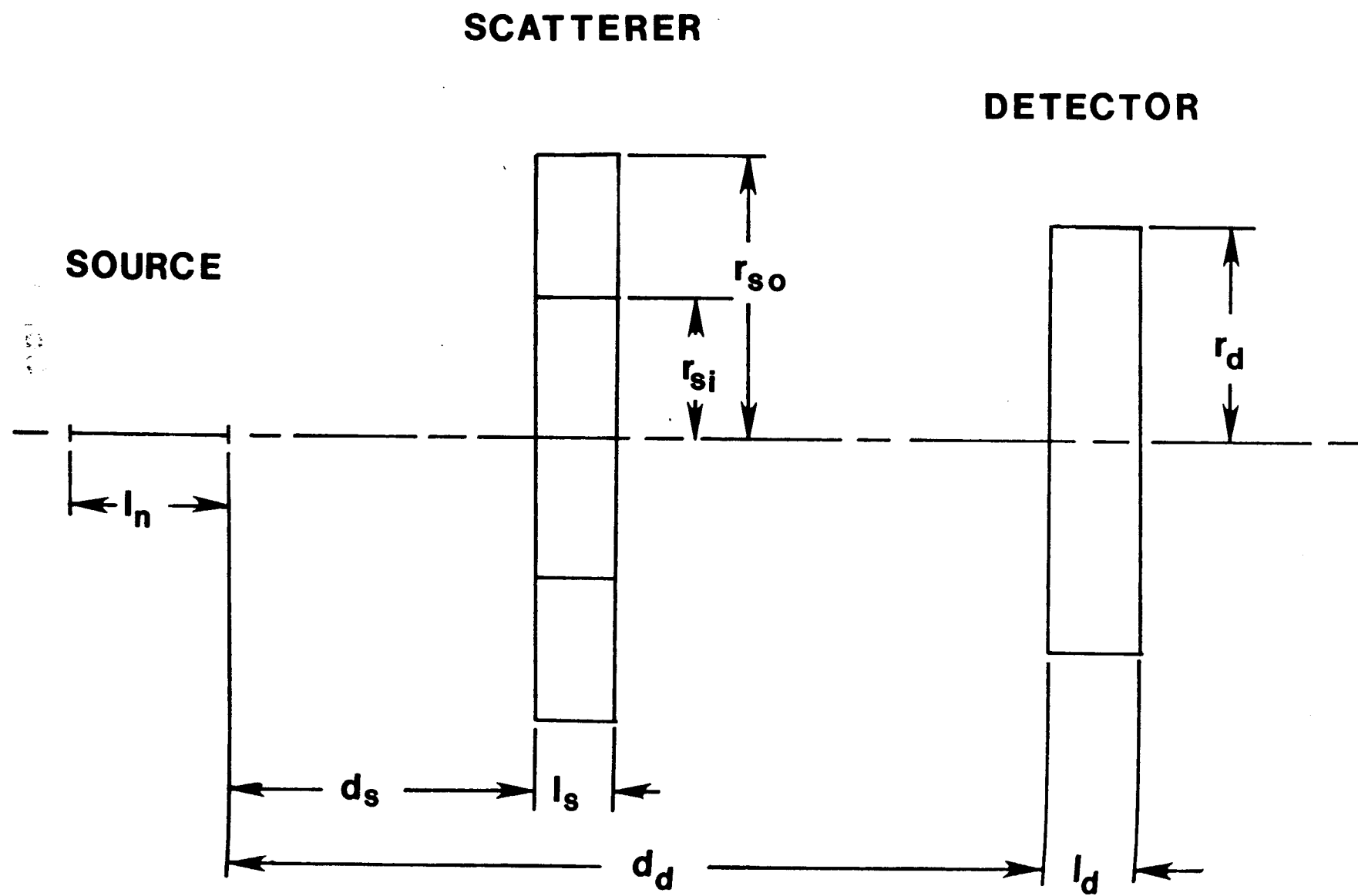


Fig. 13